Egyptian Journal of Cell and Tissue Research
Print ISSN: 2812-5436 / Online ISSN: 2812-5444

Histological Study on the Possible Protective Effect of Pumpkin Seed Oil on Cyclophosphamide Induced Hemorrhagic Cystitis in Adult Male Albino Rat

Asmaa Mohamed ElHeety [1], Esam Mohammed Elshwaihy [2], Thoraya Abd El-Aziz El-deeb [3], Maram Mohamed Elkelany [4]

[1] *Demonstrator of Histology and Cell Biology Department, Faculty of Medicine, Tanta University, Tanta, 31527, Egypt.*

[2] *Assistant Professor of Histology and Cell Biology Department, Faculty of Medicine, Tanta University, Tanta, 31527, Egypt.*

[3] *Professor of Histology and Cell Biology Department, Faculty of Medicine, Tanta University, Tanta, 31527, Egypt.*

[4] *Lecturer of Histology and Cell Biology Department, Faculty of Medicine, Tanta University, Tanta, 31527, Egypt.*

Abstract:

Background: Cyclophosphamide (CYP) is an alkylating drug used in cancer treatment, one of its common complications is hemorrhagic cystitis (HC). Pumpkin seed oil (PSO) is a strong anti-inflammatory, antioxidant and anticancer. **Aim of the Work:** This study was carried out to study the possible protective effect of pumpkin seed oil on cyclophosphamide induced hemorrhagic cystitis. **Materials & Methods:** The present study was carried out on 45 adult male albino rats. They were randomly divided into four main groups. Group I represented the control group. Group ll (PSO) received PSO at a dose of (40mg/kg/day) orally for 28 days**.** Group lll (HC) received CYP solution (75 mg/kg) for induction of HC. Group IV (PSO+HC) received PSO for 28 days as in group II, and at the 20th day, HC was induced by the same dose and manner as in group III. The urinary bladder specimens were processed for different histological techniques. Morphometrical and statistical studies were also performed. **Results:** Group III showed a lot of changes at the level of light microscopic study including epithelial ulceration, nuclear changes, hemorrhage, extensive fibrosis in Masson Trichrome stained sections

and weak PAS reaction. Furthermore, HC group showed strong positive immune reaction in the Bax immunostained sections. These findings were confirmed in our morphometric data. Additionally, ultrastructural examination of HC group showed rarefied cytoplasm, widening of intercellular spaces and swollen mitochondria. Meanwhile, group IV showed marked improvement of the previously mentioned pathological changes. **Conclusion:** PSO administration plays a protective role in cyclophosphamide-induced hemorrhagic cystitis.

Running title: PSO can suppress hemorrhagic cystitis.

Keywords: Cyclophosphamide, PSO, urinary bladder, Bax, ultrastructure.

1. Introduction:

Cyclophosphamide (CYP) is a drug that has been proved to be efficient in various human malignancies. It is also used in certain non-neoplastic conditions, such as nephrotic syndrome, rheumatoid arthritis, and systemic lupus erythematosus. Cyclophosphamide metabolites (acrolein, phosphoramide mustard) cause apoptosis and necrosis by cross-linking in the DNA. Clinical use of CYP is complicated with serious urological side effects, including voiding disturbances, urothelial damage, and hemorrhagic cystitis (HC) which is an inflammatory condition characterized by complex symptoms, such as increased urine frequency, urgency and nocturia.[1,2,3]

Pumpkin seed oil has many health benefits such as antioxidant, cytoprotective, anti-atherogenic, hepatoprotective, antidiabetic, anti-inflammatory, antibacterial, antihypertensive, antiarthritic, antidepressant, antihyperlipidemic and anticancer. The main ingredients of PSO are carotenoids, vitamin E and vitamin A.[4,5]

For all previous criteria of pumpkin seed oil, the current study was designed to evaluate its possible protective effect against cyclophosphamide induced hemorrhagic cystitis.

2. Material And Methods:

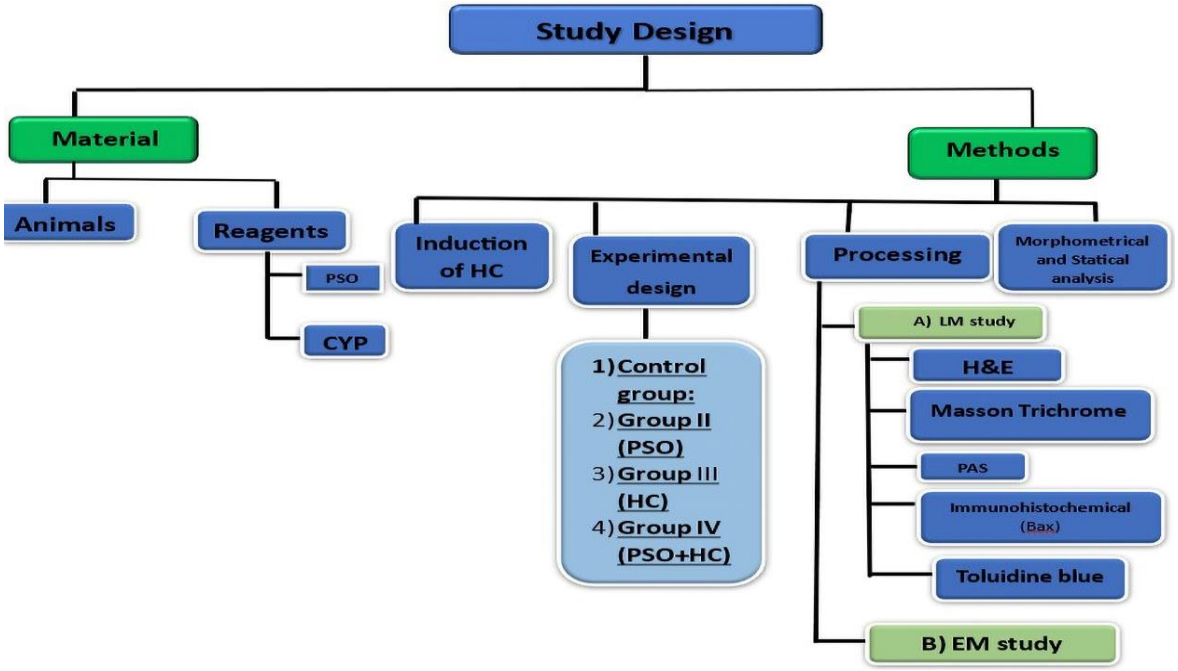

I)-Materials

Animals

This study was carried out on 45 adult male albino rats (aged; 12-14 weeks) of average weight of 150-200 gm. All the animals were housed in suitable clean properly ventilated cages under the same conditions and were fed on a similar commercial laboratory diet and water. They were acclimatized to their environment at least one week before starting the experiment. This experiment was approved by the local ethical Committee of Faculty of Medicine, Tanta University, Egypt, with the ethical code (approval code: 36180/12/22).

Reagents

- Cyclophosphamide (CYP) was obtained in the form of powder called Endoxane, (baxter oncology, Germany). CYP vial contains 1 gm powder. The required dose per rat was achieved by dissolving each vial (1 gm) in 67 ml saline.

- Pumpkin seed oil (PSO) was purchased from a local pharmacy in Tanta, in the form of capsule called Pepon (Mepaco-Arab company, Egypt) containing 300mg of PSO. It was dissolved in dimethyl sulfoxide (DMSO). The required dose per rat was achieved by

dissolving 0.7 ml of PSO in the 4.3 ml of DMSO.

II-Methods:

Induction of HC:

Hemorrhagic cystitis (HC) was induced by injecting 1ml of CYP solution intraperitoneally at 5 doses, each dose was (75 mg/kg) separated by 48 hours.[6]

Experimental design:

Animals were randomly subdivided into four main groups:

- ***Group I (control group):*** This group included 15 rat that were subdivided into three equal subgroups:
  - *Subgroup IA*: Rats were kept without any treatment.
  - *Subgroup IB*: Each rat was intraperitoneally injected by 1 ml saline, (solvent for cyclophosphamide), five times separated by 48 hours.
  - *Subgroup IC*: Each rat received 1ml per day of dimethyl sulfoxide (DMSO) (solvent for PSO), orally by gastric tube for 28 days.
- ***Group II (PSO):*** It included 10 rats, each rat received 1ml of PSO solution at a dose of (40mg/kg/day) orally by gastric tube for 28 days.[7]
- ***Group III (HC):*** It included 10 rats, that were used as model for induction of HC as described above.[6]
- ***Group IV (PSO +HC):*** It included 10 rats, each rat received PSO for 28 days as in group II, and at the 20th day, HC was induced by the same dose and manner as in group III.

The rats of subgroup IB and group III were sacrificed on the 11th day, while rats of subgroups (IA, IC), group II & group IV were sacrificed on the 29th day. Anesthesia was performed by intraperitoneal injection of sodium pentobarbital (50 mg/Kg).[8] An incision was made in the abdominal wall and urinary bladder was dissected and washed with saline. Specimens from urinary bladder were processed for light and electron microscopic examination as they were taken immediately.

Processing for light microscopy

The samples from the urinary bladder were immediately fixed in 10% formaldehyde saline solution for 24 hours, dehydrated in increasing concentration of graded alcohol, then cleared in two changes of xylol. After being impregnated in pure soft paraffin for two hours at 55°C, the specimens were then embedded in hard paraffin. Lastly, sections of 5 micron-thickness were cut using a rotatory microtome

(Leica Biosystems, China) for histological analysis. The sections were stained with hematoxylin and eosin (H&E), Masson trichrome stain and Periodic Acid Schiff (PAS) with hematoxylin as a counter stain.[9]

Some specimens were used for immunohistochemical staining to demonstrate the apoptotic changes. Tissue sections were deparaffinized and rehydrated. Antigen retrieval was carried out by heating in sodium citrate buffer (pH 6.0) for suppression of the endogenous peroxidase enzyme activity was done by 3% hydrogen peroxide/methanol .The sections were then washed three times in phosphate-buffered saline (PBS) after being incubated in 5% human serum albumin (blocking protein) for 30 minutes. The sections were then incubated overnight at 4°C with rabbit anti-Bax primary antibodies (A19684 monoclonal antibody was purchased from ABclonal Medical Company) at dilution of 1:100. The sections were washed three times in PBS and incubated in biotinylated anti-rabbit secondary antibody for 30 minutes. In addition to that, they were incubated for one hour with peroxidase-labelled streptavidin. Diaminobenzidine (DAB) was used to visualize the reaction and hematoxylin was used for counterstaining before mounting. Positive control for sections was from the human colon carcinoma. In the negative control section**,** the same method was applied with replacement of the primary antibody with Phosphate Buffer Solution. The positive immunoreactivity appeared as brown cytoplasmic reaction in the immunoreactive cells.[10,11,12]

Preparation for electron microscopic examination

The samples were quickly fixed in 2.5% phosphate buffered glutaraldehyde (pH 7.4), then the specimens were post-fixed in 1% phosphate buffered osmium tetroxide. Dehydration was done by using ascending grades of alcohol. Each specimen was placed at the tip of individually labelled capsules filled with a fresh epoxy resin mixture. Sections (1 µm thick) were cut using a LEICA ultramicrotome. In addition to that, they were stained with toluidine blue for light microscopic examination. The specimens were twice stained, first through uranyl acetate solution. Then, they were counter-stained with lead citrate. The specimens were then studied and captured on camera using (JEOL-JEM-100 SX electron microscope, Japan) at The Electron Microscopic Unit, Faculty of Medicine, Tanta University.[13]

Morphometric study:

A light microscope (Leica DM500, Switzerland) connected to a digital camera (Leica ICC50, Switzerland) was used to obtain images at the Histology department, Faculty of Medicine, Tanta University. Ten separate non-overlapping randomly selected fields from each slide of each group were examined at a magnification of 400 to quantitatively evaluate the following measurements using image J software (National Institute of Health, Bethesda, Maryland, USA):

1) The mean area percentage of the collagen fibers (Masson's Trichrome stained sections).[14]
2) The mean area percentage of PAS-stained sections. [15]
3) The mean color intensity of Bax immunostained section.[10]

Statistical Analysis:

The estimated numbers were compared, and statistical analyses were performed using one-way analysis of variance (ANOVA) and Tukey's test for group comparison by using Graph pad prism 7 (Graph pad Software, Inc.). The mean and standard deviation were used to express all the data. If the probability P-value was less than 0.05, the differences were considered significant, and if the P-value was less than 0.001, the differences were considered extremely significant.[16]

3. Results:

In the present work, all subgroups of control (IA, IB, IC) and group II (PSO group) showed the same histological results and statistical analysis.

Light microscopic results:

I) Hematoxylin and eosin-stained sections:

Examination of sections obtained from the urinary bladder of the control showed the known histological structure of the urinary bladder. The mucosa of the urinary bladder was highly folded. It was formed of the (urothelium & Lamina propria) **(Fig.1-A**). The urothelium was formed of transitional epithelium that was intact and continuous layer, it was about 3-5 layers. The superficial layer was formed of umbrella or dome-shaped cells **(Fig.1-B**). The lamina propria contained blood vessels**.** The muscle layer was composed of interlaced muscle bundles. The muscle fibers ran irregularly in all directions **(Figs.1-C&D**).

Light microscopic examination of H&E-stained sections of the urinary bladder of group III showed loss of the urothelial continuity with desquamated cells into the lumen and focal ulcerated

areas. Additionally, thinning of epithelium with areas of focal loss or even extensive damage of epithelium was observed. Meanwhile, lamina propria showed denuded areas, apparent very wide space, severe interstitial hemorrhage and dilated congested blood vessels with interruption of its endothelial lining **(Fig.2-A,B,C,D&E**). Besides that, vacuolated epithelial cells, ballooning of some of them, noticeable separation and appearance of spaces between them were detected. Furthermore, nuclear changes in the form of dark, shrunken and fragmented nuclei were observed. Some surface epithelial cells showed hyper eosinophilia, while the others appeared with squamous cell lining **(Fig.3-A&B**). In addition to that, focal disrupted basement membrane was noticed **(Fig.3-C**). Moreover, widely separated muscle bundles were also detected with presence of vacuolation in the muscle fibers. Meanwhile, mononuclear cellular infiltration in lamina propria and interstitial hemorrhage between muscle fibers were also observed **(Fig.3-D).**

Additionally, some areas in the urothelium revealed proliferation of the cell layers with fading of nuclei (karyolysis) **(Fig.4-A)**, other areas revealed presence of blood vessels (neovascularization) in the urothelium. Furthermore, nuclear changes in the form of dark, shrunken (pyknosis) and fragmented nuclei (karyorrhexis) were observed **(Fig.4-B).** Moreover, loss of demarcation between the urothelium and the lamina propria with absence of the basement membrane were noticed **(Fig.4-C).** Furthermore, lamina propria revealed blood vessels with vacuolated smooth muscle cells of its tunica media **(Fig.4-D).**

Urinary bladder sections of the PSO-HC group (group IV) showed that epithelium appeared near normal, with apparent superficial dome-shaped cells. Cytoplasmic vacuolations were also noticed. The lamina propria revealed congested blood vessels **(Fig.5-A&B)**. Moreover, the muscle fibers showed some vacuolations **(Fig.5-C)**.

II)Masson trichrome stain:

Masson trichrome-stained sections of the control groups showed apparent mild deposition of blue collagen fibers in the lamina propria and in-between the muscles **(Figs.6-A&B)**. Meanwhile, Masson trichrome-stained sections of group III showed apparent extensive deposition of blue collagen fibers in the lamina propria and in between the muscles **(Figs.6-C&D)**. Furthermore, Masson trichrome-stained sections of this group showed apparent mild

deposition of blue collagen fibers in the lamina propria and in between the muscles **(Figs.6-E&F)**.

III)Periodic acid Schiff's reaction (PAS) stain:

PAS-stained sections of the control group showed strong PAS-positive reaction of both the glycosaminoglycan (GAG) layer of the urothelium which appeared as continuous layer on the luminal surface of the urothelium and in the urothelial basement membrane **(Fig.7-A)**. PAS-stained sections of the HC group showed an apparently weak PAS reaction, with discontinuous GAG layer on the luminal surface of some areas of the urothelium. Furthermore, there was interruption of the urothelial basement membrane **(Fig.7-B)**. PAS-stained sections of the PSO-HC group showed apparent moderate PAS reaction, with intact GAG layer on the luminal surface of the urothelium. Moreover, PAS reaction was noticed at the urothelial basement membrane **(Fig.7-C)**.

IV) Immunohistochemical staining:

All immunostained sections from control group revealed apparent weak positive immune reaction for bax in the cytoplasm of many urothelial cells (**Fig.8-A)**. Immunostained sections from the HC group revealed an apparent strong positive immune reaction for bax in the cytoplasm of many urothelial cells **(Fig.8-B).** Immunostained sections from PSO-HC group revealed an apparent moderate positive immune reaction for bax in cytoplasm of many urothelial cells (**Fig.8-C)**.

V) Toluidine blue stain:

Sections of the control group stained with toluidine blue showed normal urothelial cells with rounded nuclei having prominent nucleoli with presence of characteristic dome-shaped cells **(Fig.9-A)**. Sections of the urinary bladder from the HC group (group III), showed urothelial cells vacuolation with shrunken and indented nuclei. Moreover, desquamated cells were noticed **(Fig.9-B)** with presence of intraepithelial mast cell infiltration stained metachromatically **(Fig.9-C)**. Examination of sections of the urinary bladder from the PSO-HC group (group IV), showed urothelial cells that appeared near normal. Cytoplasmic vacuolations were also noticed **(Fig.9 - D)**.

Morphometric and statistical analysis results:

The mean area percentage of collagen fibers in the HC group (group III) showed an extremely significant increase compared with the control

group. PSO-HC group (group IV) showed a non-significant increase compared with control group (group I). All these data illustrated in table (1) and **(Fig.10-A).**

The mean area percentage of PAS-stained sections in the HC group (group III) showed an extremely significant decrease compared with the control group. PSO-HC group (group IV) showed a highly significant decrease compared with control group (group I). All these data were illustrated in table (2) and **(Fig.10-B).**

The mean color intensity of Bax immunostained sections in the HC group (group III) showed an extremely significant increase compared with control group. PSO-HC group (group IV) showed a significant increase compared with control group (group I). All these data illustrated in table (3) and **(Fig.10-C).**

Table (1): The mean area percentage of the Masson Trichrome-stained sections of the urinary bladder.

Area %	**Group I**	**Group II (PSO)**	**Group III (HC)**	**Group IV (PSO-HC)**
Range	12-15.12	12-15.4	32.673-40.446	12.378-15.687
Mean ± SD	13.5296±0.8722	13.6843±1.18	37.1402±2.833	14.0872±0.9284
ANOVA				
P-value	<.0001***			
Tukey test				

P-value	Control &HC (I & III)	Control & PSO (I & II)	PSO & HC (II & III)	HC & PSO-HC (III & IV)	Control & PSO-HC (I & IV)	PSO & PSO-HC (II & IV)
	<.001***	>.05	<.001***	<.001***	>.05	>.05

SD: standard deviation ***extremely significant

Table (2): The mean area percentage of the PAS-stained sections of the urinary bladder.

Area %		Group I	Group II (PSO)	Group III (HC)	Group IV (PSO-HC)	
Range		25.31-38.111	25.31-35	5.395-10.408	25.99-29.2	
Mean ± SD		32.1706±4.542	31.9289±2.859	7.3785±1.634	27.4705±1.407	
ANOVA						
P-value		<.0001***				
Tukey test						
P-value	control & HC (I & III)	control & PSO (I & II)	PSO & HC (II & III)	HC & PSO-HC (III & IV)	control & PSO-HC (I & IV)	PSO&PSO-HC (II & IV)
	<.001* **	**>.05**	**<.001*** **	**<.001*** **	**<.01** **	**<.01** **

SD: standard deviation ***extremely significant
** Highly significant

Table (3): The mean color intensity of the Bax-stained sections of the urinary bladder.

Color intensity		Group I	Group II (PSO)	Group III (HC)	Group IV (PSO-HC)	
Range		12-18.394	12.8-17.3	47.032-55.19	14-20.7	
Mean ± SD		15.5743±2.274	15.5299±1.568	52.07±2.541	18.6453±2.175	
ANOVA						
P-value		<.0001***				
Tukey test						
P-value	control &HC (I & III)	Control & PSO (I & II)	PSO & HC (II & III)	HC & PSO-HC (III& IV)	Control & PSO-HC (I & IV)	PSO& PSO-HC (II & IV)
	<.001* **	**>.05**	**<.001*** **	**<.001*** **	**<.05***	**<.05***

SD: standard deviation ***extremely significant
* Significant

Electron microscopic study:

Electron microscopic examination of the urothelium from control group revealed oval to round nucleus with a prominent nucleolus and extended chromatin **(Fig.11-A)**., some cells revealed nucleus with two prominent nucleoli, while the cytoplasm showed normal pleomorphic mitochondria and normal RER. Irregular dense plaques at the apical surfaces with normal characteristic angular contour were prominent. Apical fusiform vesicles were also observed. Additionally, intact intercellular junctions formed of zonula occludens, zonula adherens and desmosome were noticed **(Fig.11-B&C)**. Additionally, basement membrane appeared continuous and corrugated **(Fig.12-A),** the lamina propria appeared with normal blood capillary **(Fig.12-B).**

Examination of ultrathin sections obtained from group III showed remarkable indented nuclei with absent nucleolus**,** while others appeared dark shrunken. The presence of RBCS & sloughed cells into the lumen were also detected. Some superficial cells appeared with rarefied cytoplasm **(Figs.13&14).** Heterogenous bodies indicating secondary lysosome were also noticed **(Fig.15-A).** Moreover, widening of intercellular space was also detected **(Fig.15-B).** Additionally, swollen mitochondria **(Fig.15-C)** and dilated RER were also observed **(Fig.15-D)**. Basement membrane appeared discontinuous **(Fig.16-A)**. Meanwhile, excessive collagen deposition **(Fig.16-B)** and large, congested blood capillary were detected in the lamina propria **(Fig.16-C).**

Examination of ultrathin sections of PSO-HC group revealed oval to round nuclei with prominent nucleolus, some of them appeared indented. Few cytoplasmic vacuolation were noticed. Apical angular contour and apical fusiform vesicles were also observed **(Fig.17-A&B).** Apparently normal RER and mitochondria were detected with near normal intercellular junction **(Fig.17-C).**

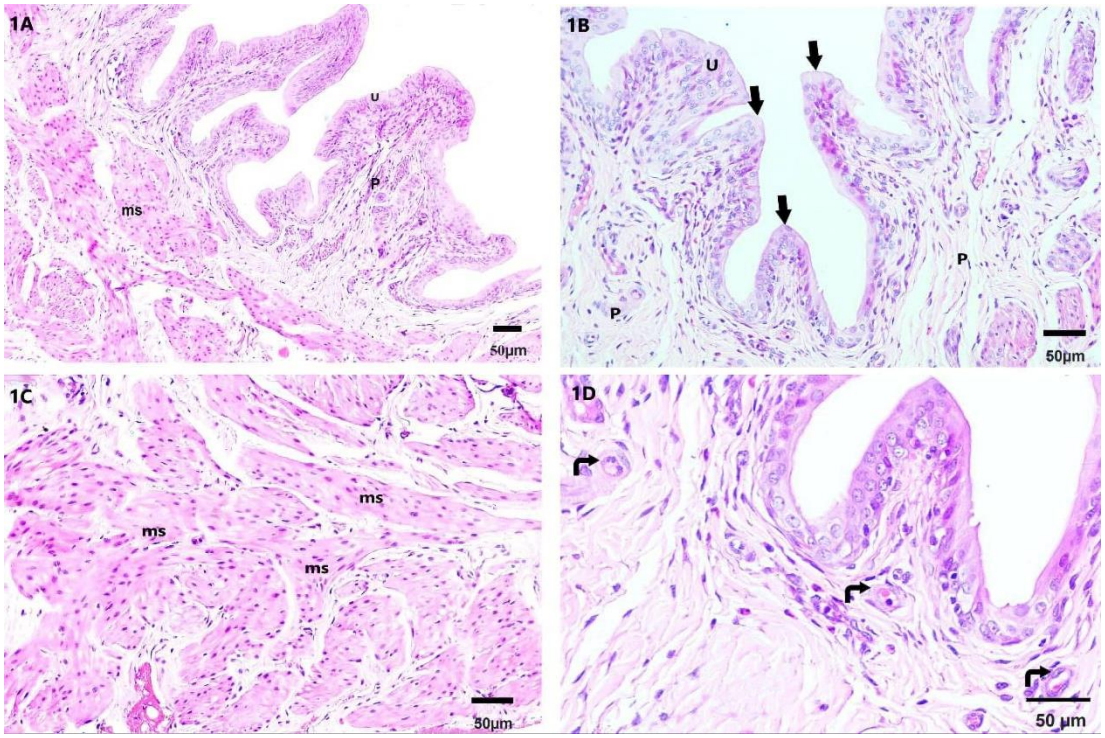

Fig. (1): A photomicrograph of a section of the urinary bladder from control group (group I) **1-A)** showing the folded mucosa composed of the urothelium **(U)** and lamina propria **(P)** with the muscle layer **(ms) (H&E x100, scale bar= 50 µm)**. **1-B)** showing the transitional epithelium formed of 3-5 layers of cells **(U)** with the superficial dome-shaped cells **(arrows) (H&E x200, scale bar= 50 µm)**. **1-C)** showing the muscle layer of the urinary bladder **(ms)** formed of interlaced bundles which are irregularly arranged **(H&E x200, scale bar= 50 µm)**. **1-D)** showing normal blood vessels **(bended arrows)** in lamina propria **(H&E x400, scale bar= 50 µm)**.

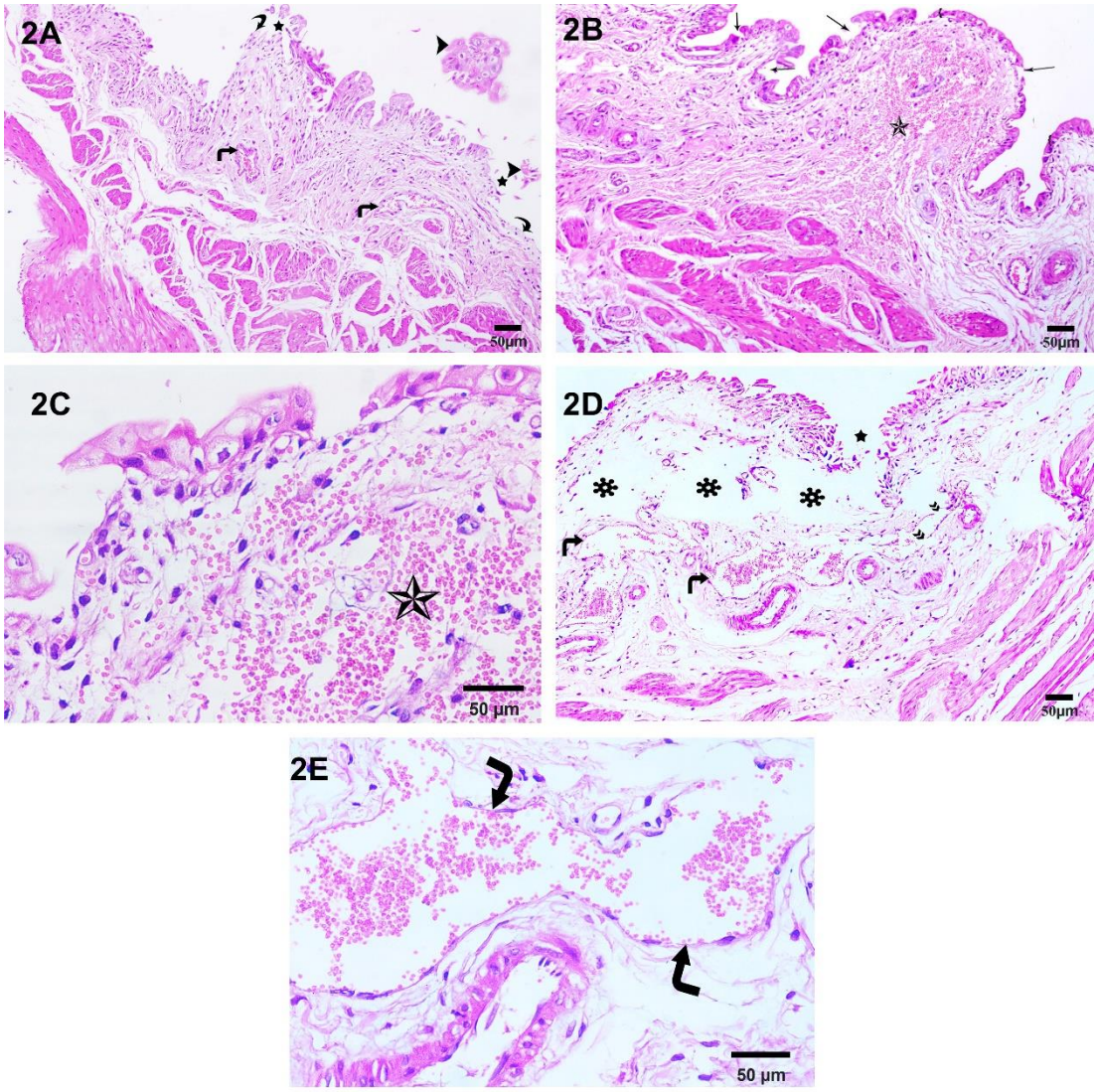

Fig. (2): A photomicrograph of a section of the urinary bladder from HC group (group III). **2-A)** showing loss of the urothelial continuity with desquamated cells into the lumen **(arrowheads)** and focal ulcerated areas **(stars)**, denuded areas of lamina propria are observed **(curved arrows)** with dilated congested blood vessels **(bended arrows)** in lamina propria **(H&E x100, scale bar= 50 µm). 2-B)** showing thinning of epithelium **({)** with areas of focal loss **(thin arrows)** with interstitial hemorrhage in lamina propria **(star) (H&E x100, scale bar= 50 µm)**. **2-C)** higher magnification of the previous figure showing severe interstitial hemorrhage **(star) (H&E x400, scale bar= 50 µm)**. **2-D)** showing extensive damage of the epithelium with ulcerated areas **(star)** with very wide spaces in lamina propria **(asteriks)**. Congested blood vessels **(bended arrows**) with interrupted endothelial lining are also noticed **(double arrow heads) (H&E x100, scale bar= 50 µm)**. **2-E)** higher magnification of the previous figure showing highly congested blood vessels **(bended arrows**) **(H&E x400, scale bar= 50 µm)**.

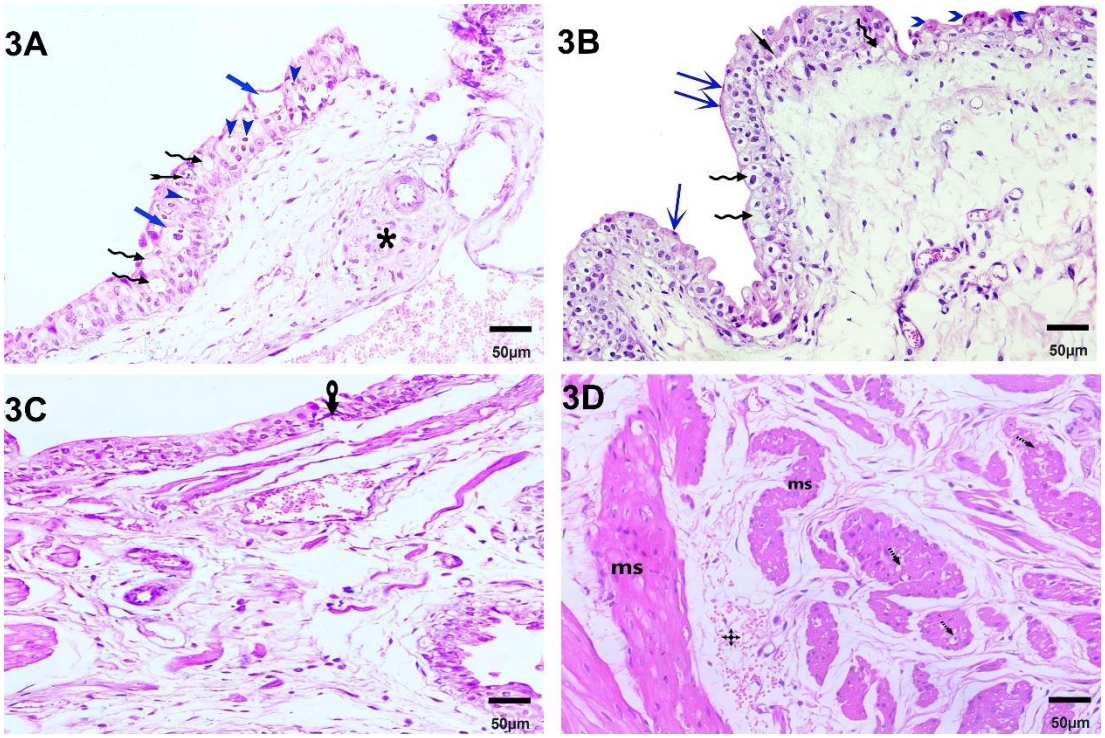

Fig. (3): A photomicrograph of a section of the urinary bladder from HC group (group III). **3-A)** showing vacuolated epithelial cells **(zigzag arrows)**. Some of them appeared ballooned **(blue arrow**). Some nuclei appear dark and shrunken **(arrowheads)**, while others appear fragmented **(bifid arrow).** Notice the mononuclear cellular infiltration **(asterisk) (H&E x200, scale bar= 50 µm). 3-B)** showing vacuolated epithelial cells **(zigzag arrows)** with appearance of space in between cells **(pointed arrows**), some surface epithelial cells showed hyper eosinophilia **(arrowheads),** while the others appeared with squamous cell lining **(blue arrows) (H&E x200, scale bar= 50 µm)**. **3-C**) showing focal disruption of the basement membrane **(arrow) (H&E x200, scale bar= 50 µm)**. **3-D)** showing widely separated muscle bundles **(ms)** with vacuolated muscle fiber **(striped arrows)** and interstitial hemorrhage **(quard arrow**) **(H&Ex200, scale bar= 50 µm)**.

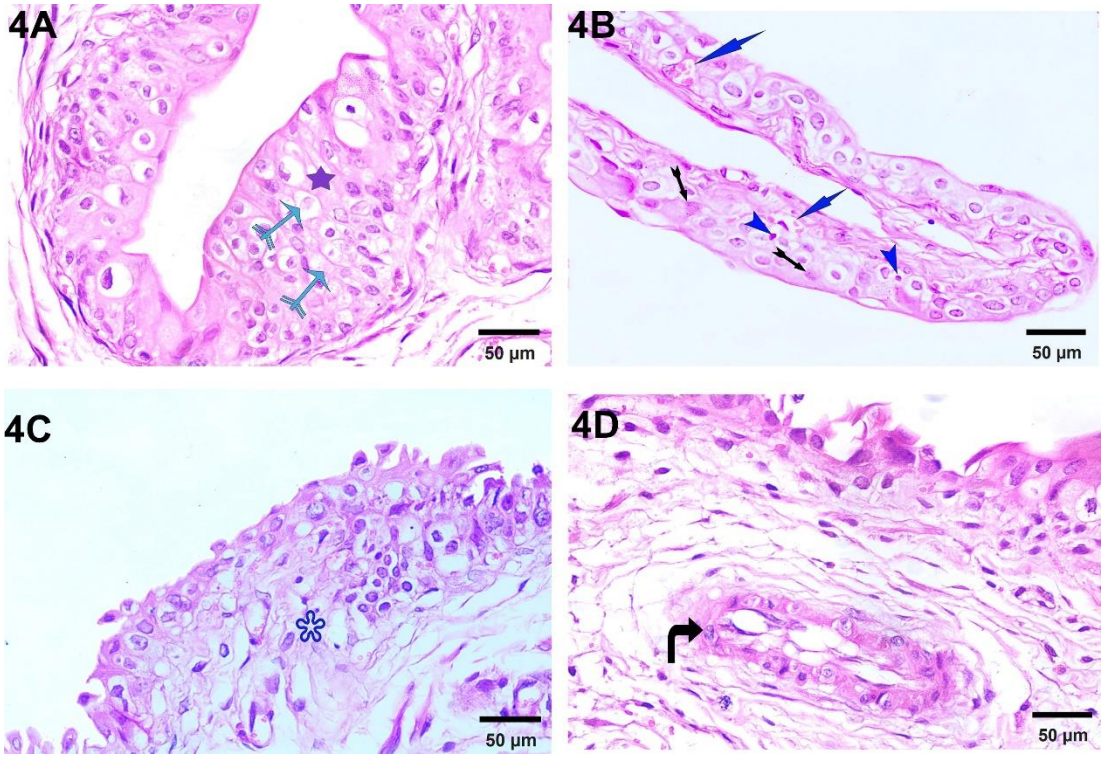

Fig. (4): A photomicrograph of a section of the urinary bladder from HC group (group III). **4-A)** showing proliferation of the urothelium **(star),** notice fading of some nuclei (karyolysis) **(H&Ex400, scale bar= 50 µm). 4-B)** showing appearance of blood vessel within the urothelium **(pointed arrows),** some nuclei appear dark and shrunken (pyknotic) **(arrowheads)**, while others appear fragmented (karyorrhexis) **(bifid arrow) (H&Ex400, scale bar= 50 µm)**. **4-C)** showing loss of demarcation between urothelium and lamina propria with absence of basement membrane **(asterik) (H&Ex400, scale bar= 50 µm)**. **4-D)** showing blood vessel with vacuolated smooth cells of its tunica media **(bended arrow) (H&Ex400, scale bar= 50 µm).**

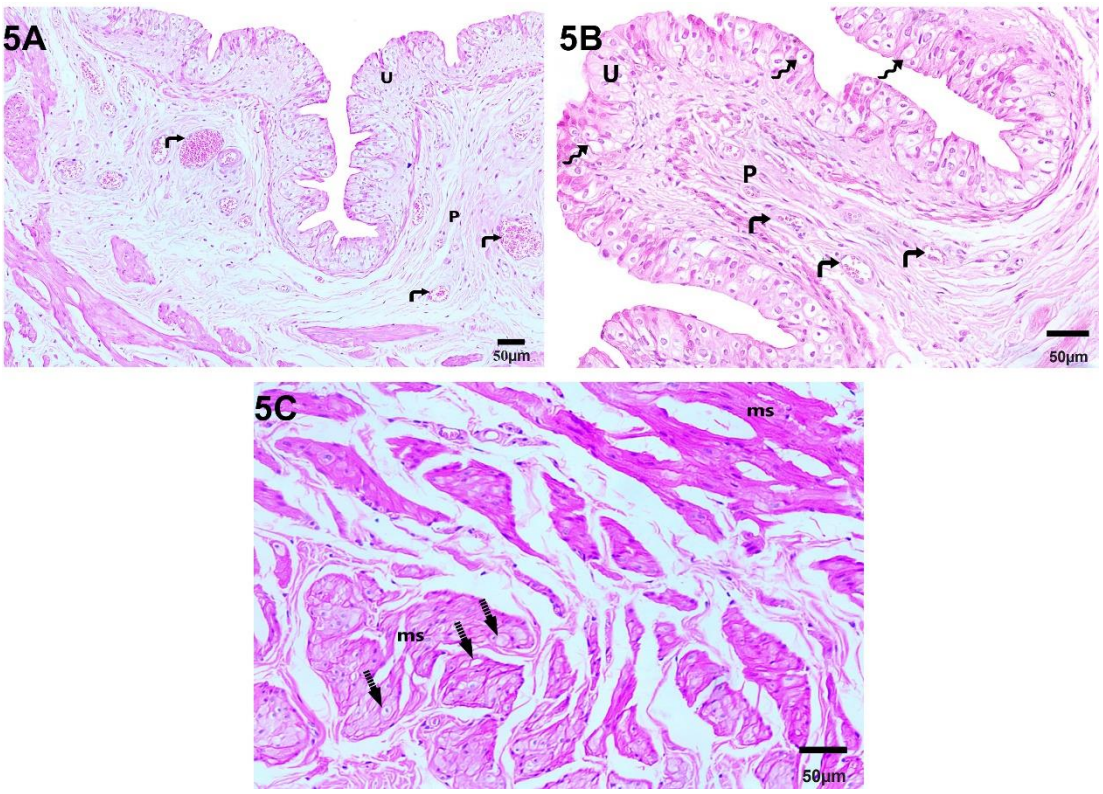

Fig. (5): A photomicrograph of a section of the urinary bladder from the PSO-HC group (group IV). **5-A**) showing epithelium appeared near normal **(U).** Notice lamina propria **(P)** with congested blood vessels **(bended arrows) (H&E x100, scale bar= 50 µm). 5-B)** showing urothelium (**U)** with cytoplasmic vacuolation **(zigzag arrows**). Notice lamina propria (**P)** with congested blood vessels **(bended arrows) (H&E x200, scale bar= 50 µm). 5-C)** showing the muscle fibers **(ms)** with some vacuolations **(striped arrows) (H&E x200, scale bar= 50 µm).**

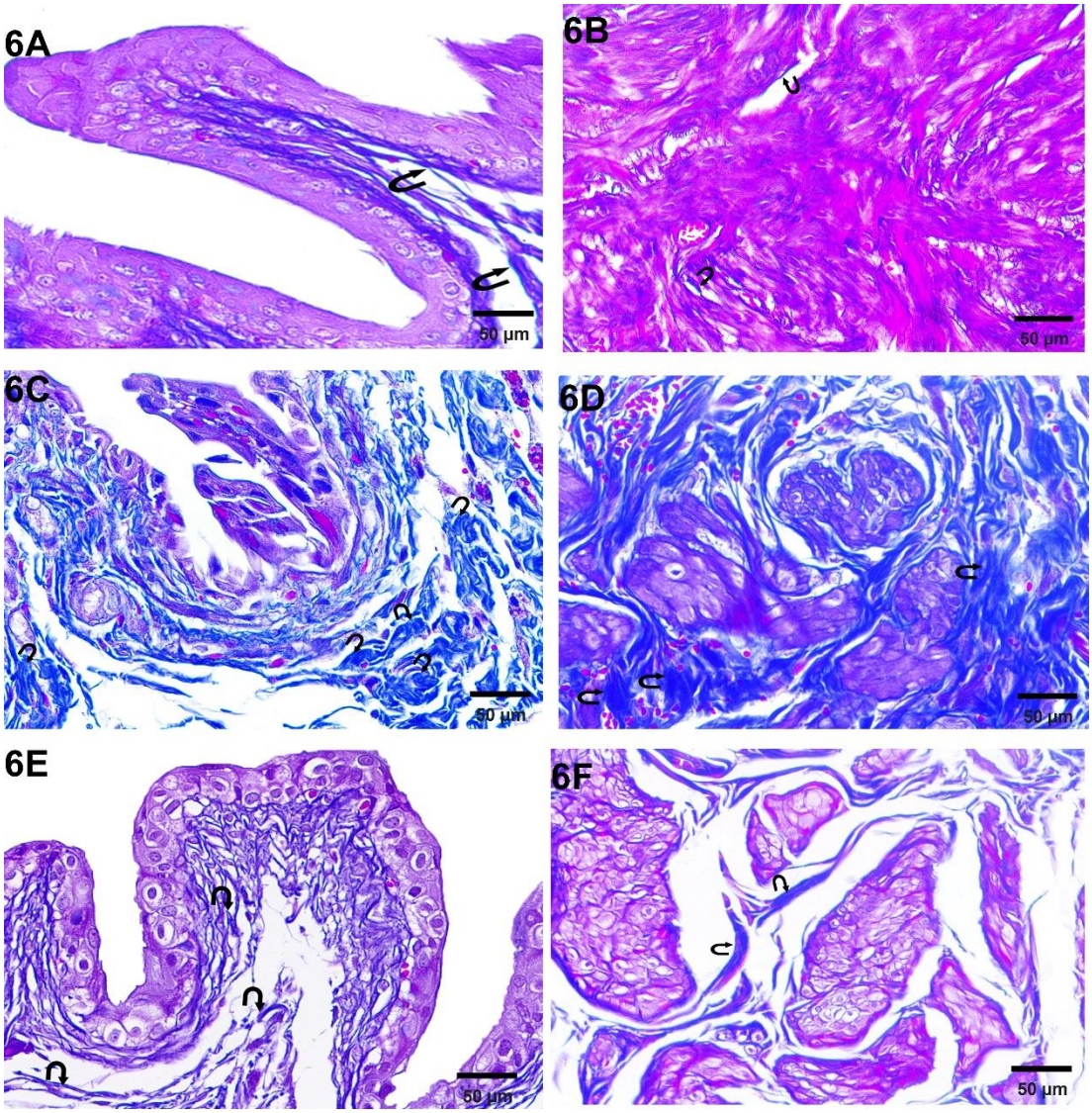

Fig. (6): 6-A) A photomicrograph of a section of the urinary bladder from the control group, showing apparent mild deposition of blue collagen fibers in the lamina propria **(curved arrows**). **6-B)** section of the urinary bladder from the control group, showing apparent mild deposition of blue collagen fibers between the muscle fibers (**curved arrows). 6-C)** section of the urinary bladder from HC group (group III), showing apparent excessive deposition of blue collagen fibers in the lamina propria **(curved arrows).6-D)** section of the urinary bladder from HC group (group III), showing apparent excessive deposition of blue collagen fibers between the muscle fibers **(curved arrows).6-E)** section of the urinary bladder from the PSO-HC group (group Iv), showing apparent mild deposition of blue collagen fibers in the lamina propria **(curved arrows).6-F)** section of the urinary bladder from the PSO-HC group (group Iv), showing apparent mild deposition of blue collagen fibers between the muscle fibers **(curved arrows). (Masson Trichrome, x 400, scale bar = 50 µm).**

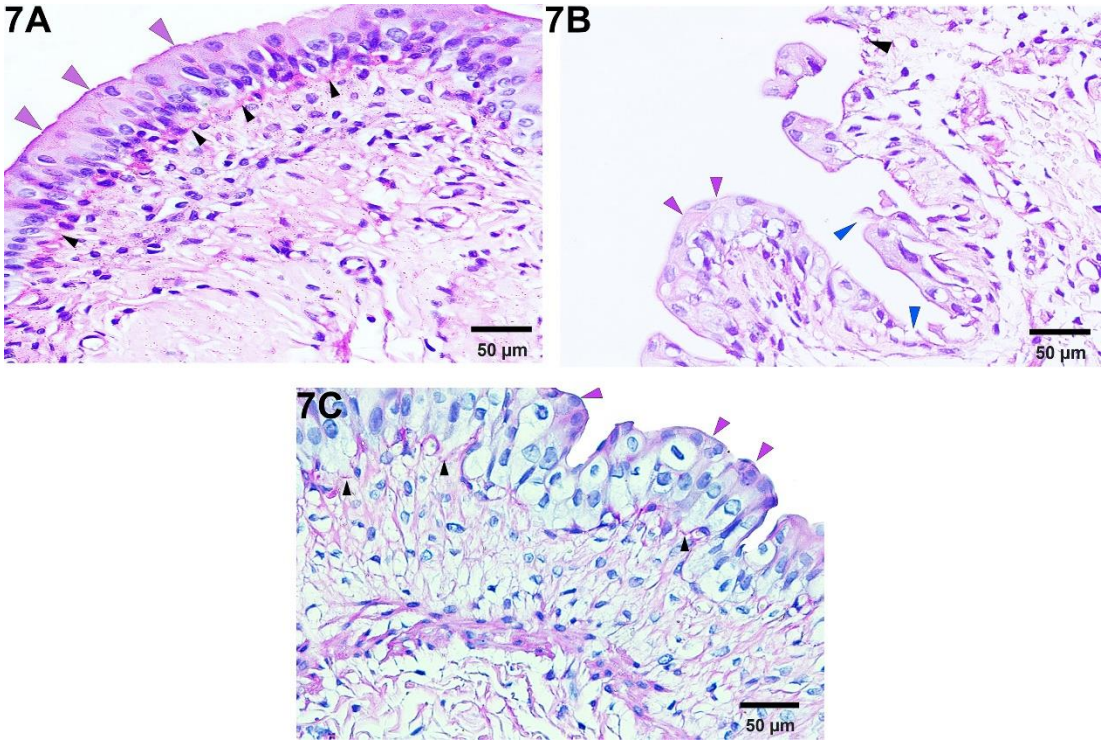

Fig. (7): 7-A) A photomicrograph of a section of the urinary bladder from control group showing strong PAS positive reaction with continuous GAG layer on the luminal surface of the urothelium (**purple arrowheads)**. Notice intact basement membrane **(black arrowheads)**. **7-B**) section of the urinary bladder from the HC group showing apparent weak PAS reaction **(purple arrowheads)** and discontinuous GAG layer on the luminal surface of the urothelium **(blue arrowheads).** Notice areas of interrupted basement membrane **(black arrowhead)**. **7-C)** section of the urinary bladder from the PSO-HC group showing apparent moderate PAS reaction and intact GAG layer on the luminal surface of the urothelium (**purple arrowheads**). Notice PAS reaction of the basement membrane (**black arrowheads**) **(PAS x400, scale bar = 50 µm).**

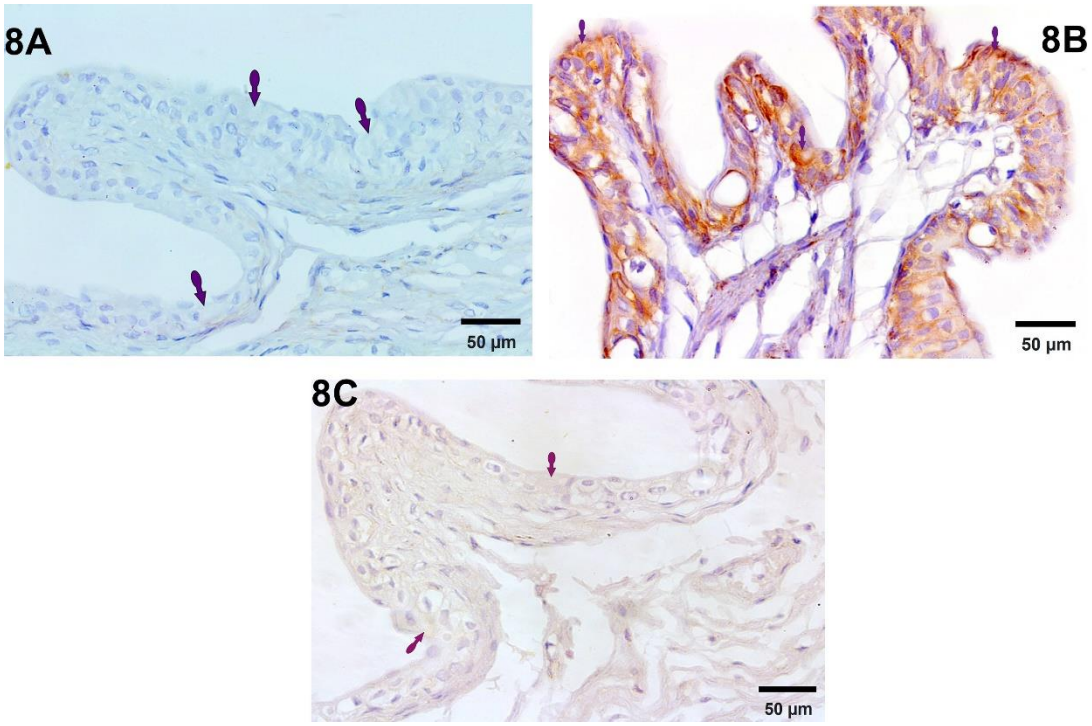

Fig. (8): 8-A) A photomicrograph of a section of the urinary bladder from control group (group I) showing apparent weak positive immune reaction for bax in the cytoplasm of many urothelial cells **(dotted arrows). 8-B)** section of the urinary bladder from the HC group showing apparent strong positive immune reaction for bax in the cytoplasm of many urothelial cells **(dotted arrows). 8-C)** section of the urinary bladder from the PSO-HC group showing apparent moderate positive immune reaction for bax in the cytoplasm of many urothelial cell **(dotted arrows) (Bax immunostaining x400, scale bar = 50 µm)**.

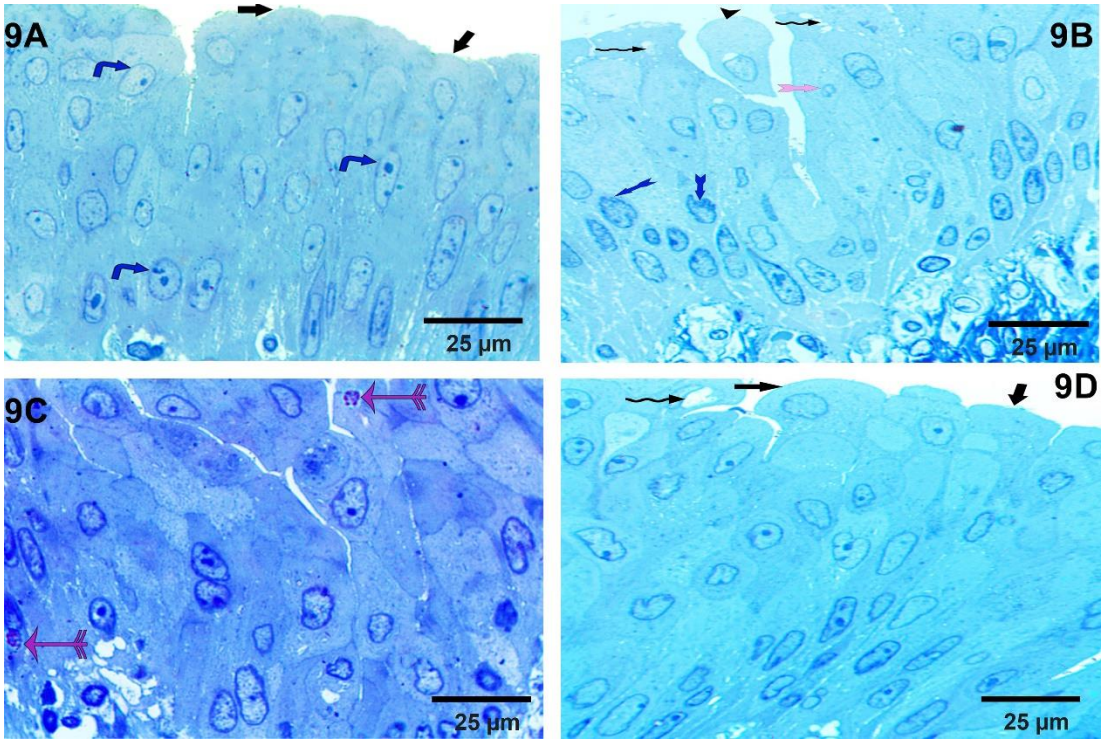

Fig. (9): **9-A**) A photomicrograph of a section of the urinary bladder from the control group (group I) showing normal urothelial cells with oval to rounded nuclei having prominent nucleoli **(bended arrows)**. Notice outer dome-shaped cells **(thick arrows). 9-B)** section of the urinary bladder from the HC group showing urothelial cells vacuolation **(zigzag arrows)** with shrunken **(purple bifid arrows)** and indented nuclei **(blue bifid arrows)**. Notice desquamated cell **(arrowhead).9-C)** section of the urinary bladder from the HC group showing intraepithelial mast cell infiltration metachromatically stained **(arrows).9-D)** section of the urinary bladder from the PSO-HC group (group IV), showing urothelial cells appeared near normal with outer dome-shaped cells **(thick arrows)**. Notice few cytoplasmic vacuolation **(curved arrow) (Toluidine blue x1000, scale bar = 25 µm).**

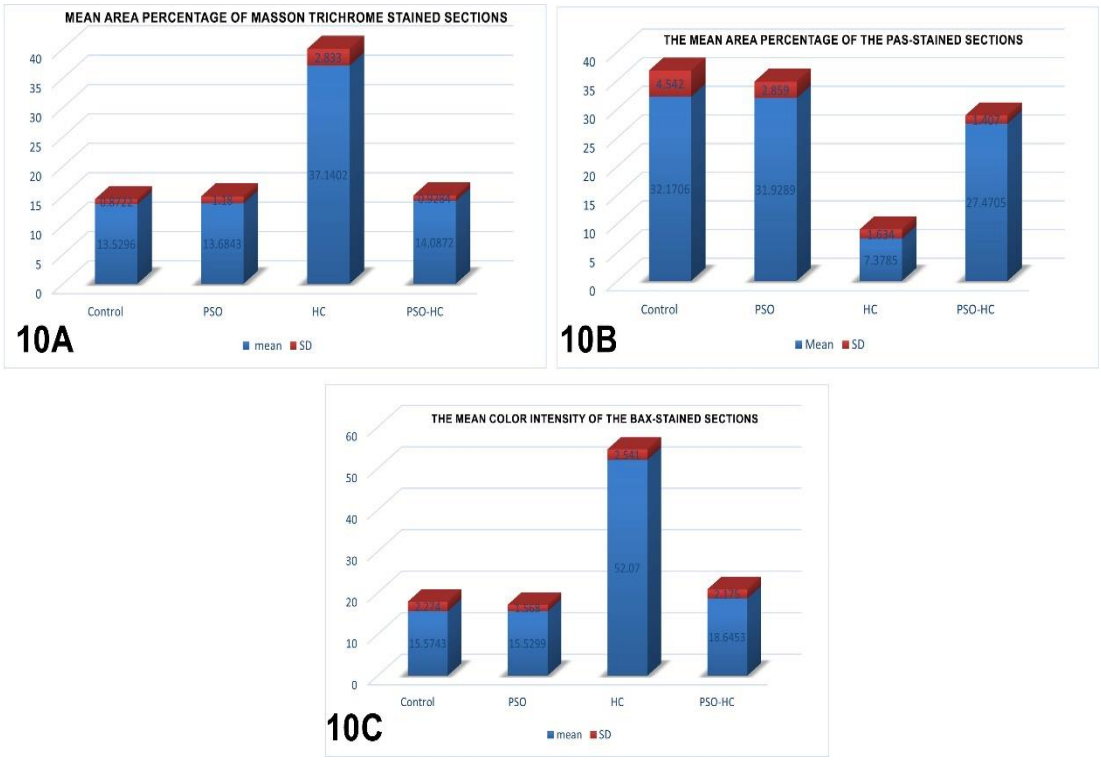

Fig. (10): Histogram-A: The mean area percentage of Masson Trichrome stained sections of the urinary bladder. Histogram-B: The mean area percentage of the PAS-stained sections of the urinary bladder. Histogram-C: The mean color intensity of the Bax-stained sections of the urinary bladder.

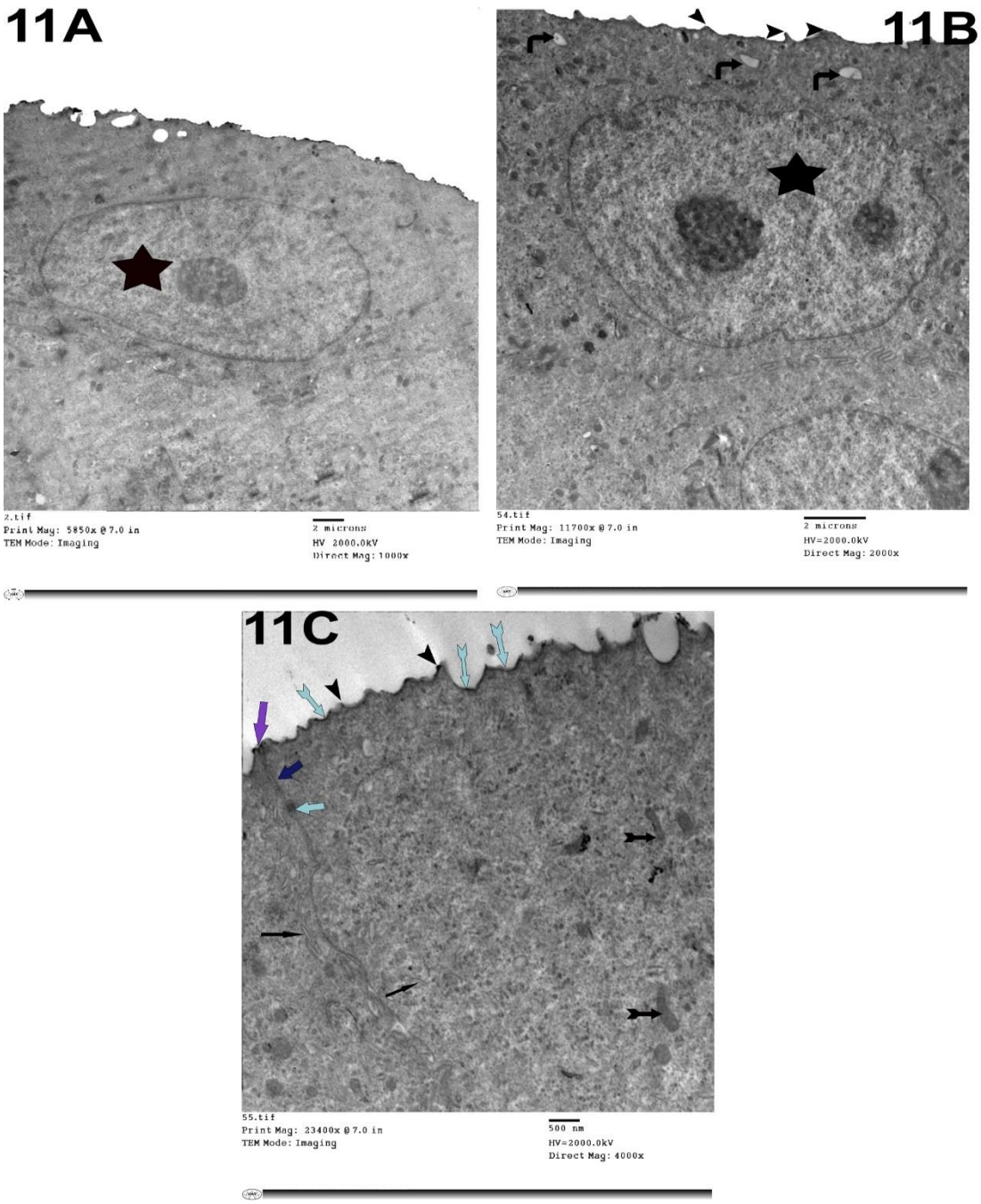

Fig. (11): An electron micrograph of the urothelium from control group: **11-A**) showing oval to round nucleus with a prominent nucleolus and extended chromatin **(star) (X 1000)**. **11-B**) showing nucleus with two prominent nucleoli **(star) (X 2000).** The apical fusiform vesicles are also observed **(bended arrows).** Notice normal angular contour **(arrow heads). 11-C)** showing the irregular dense plaques at the apical surfaces **(green bifid arrows)** with the characteristic angular contour **(arrow heads**) and intact intercellular junctions formed of zonula occludens **(purple arrow)**, zonula adherens **(blue arrow)** and desmosome **(green arrow)**. The cytoplasm contains normal pleomorphic mitochondria **(black bifid arrows)** with normal RER **(black arrows) (X 4000)**.

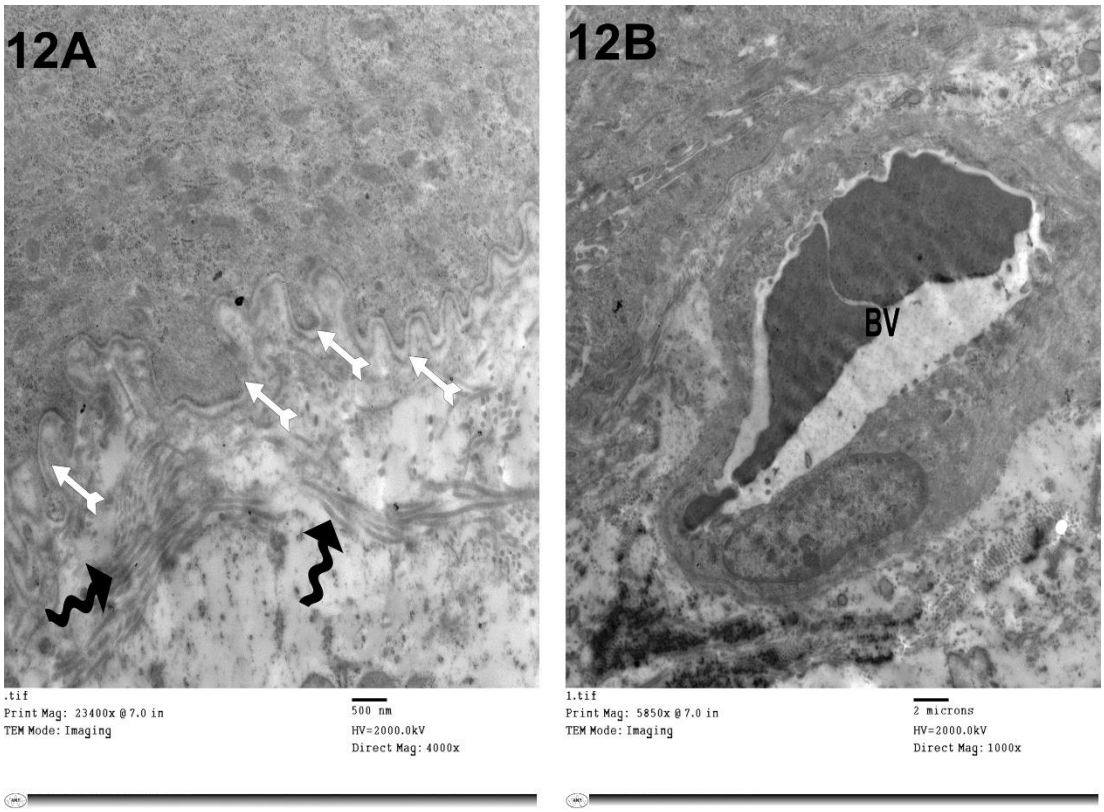

Fig. (12): An electron micrograph of the urothelium from control group: **12-A**) showing continuous corrugated basement membrane **(white bifid arrows),** notice the arrangement of collagen fibers **(zigzag arrows) (X 4000)**. **12-B**) showing the lamina propria appeared with normal blood capillary **(BV) (X 1000)**.

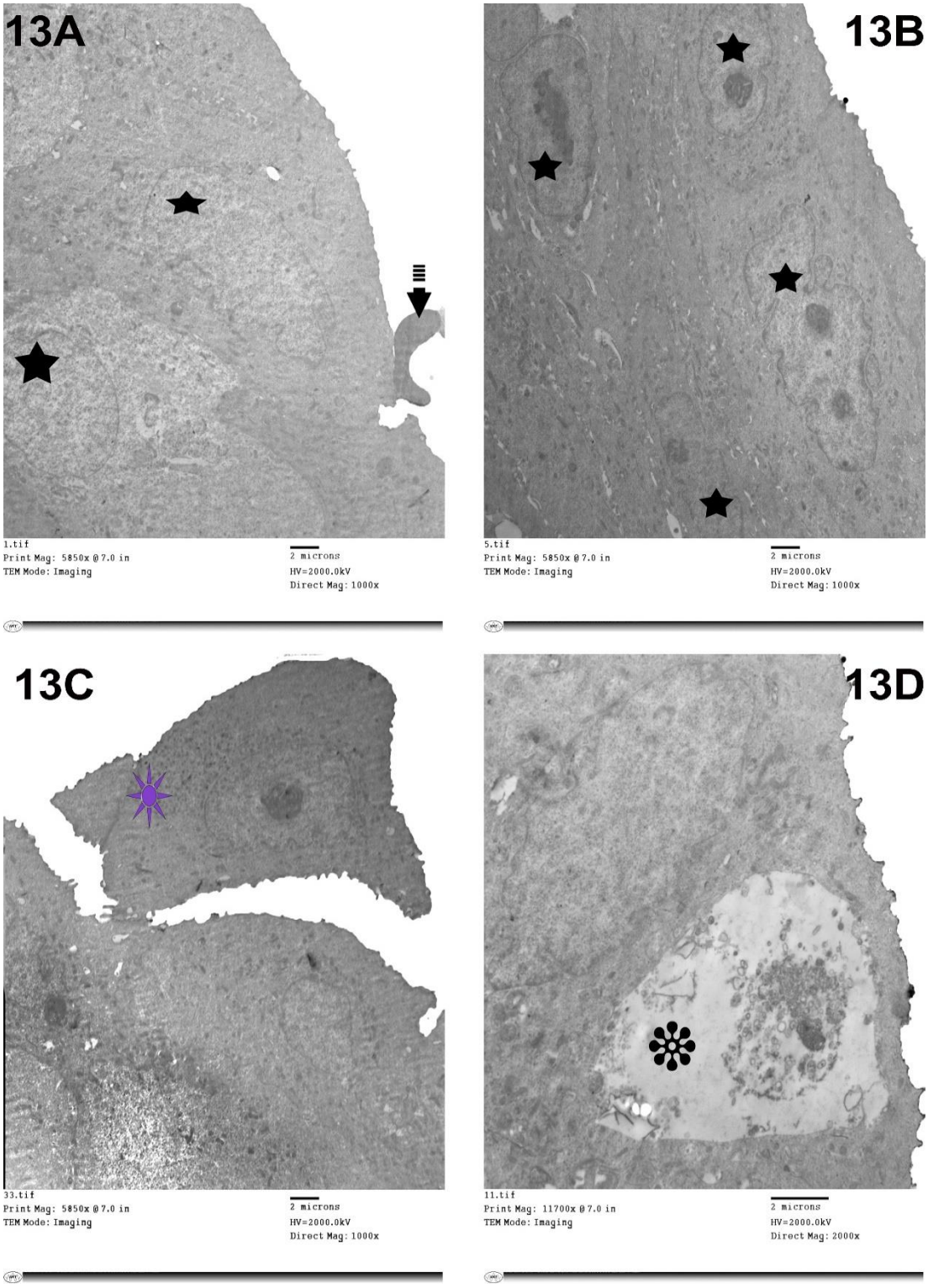

Fig. (13): An electron micrograph of the urothelium from HC group. **13-A**) showing indented nucleus **(star)**with absent nucleolus. Notice presence of RBCS in the bladder lumen **(black stripped arrow)**. **13-B)** showing highly indented nuclei **(stars). 13-C**) showing a sloughed cell into the lumen of the bladder (purple star) **(X 1000)**. **13-D)** showing superficial cell with rarefied cytoplasm **(asterisk) (X 2000)**.

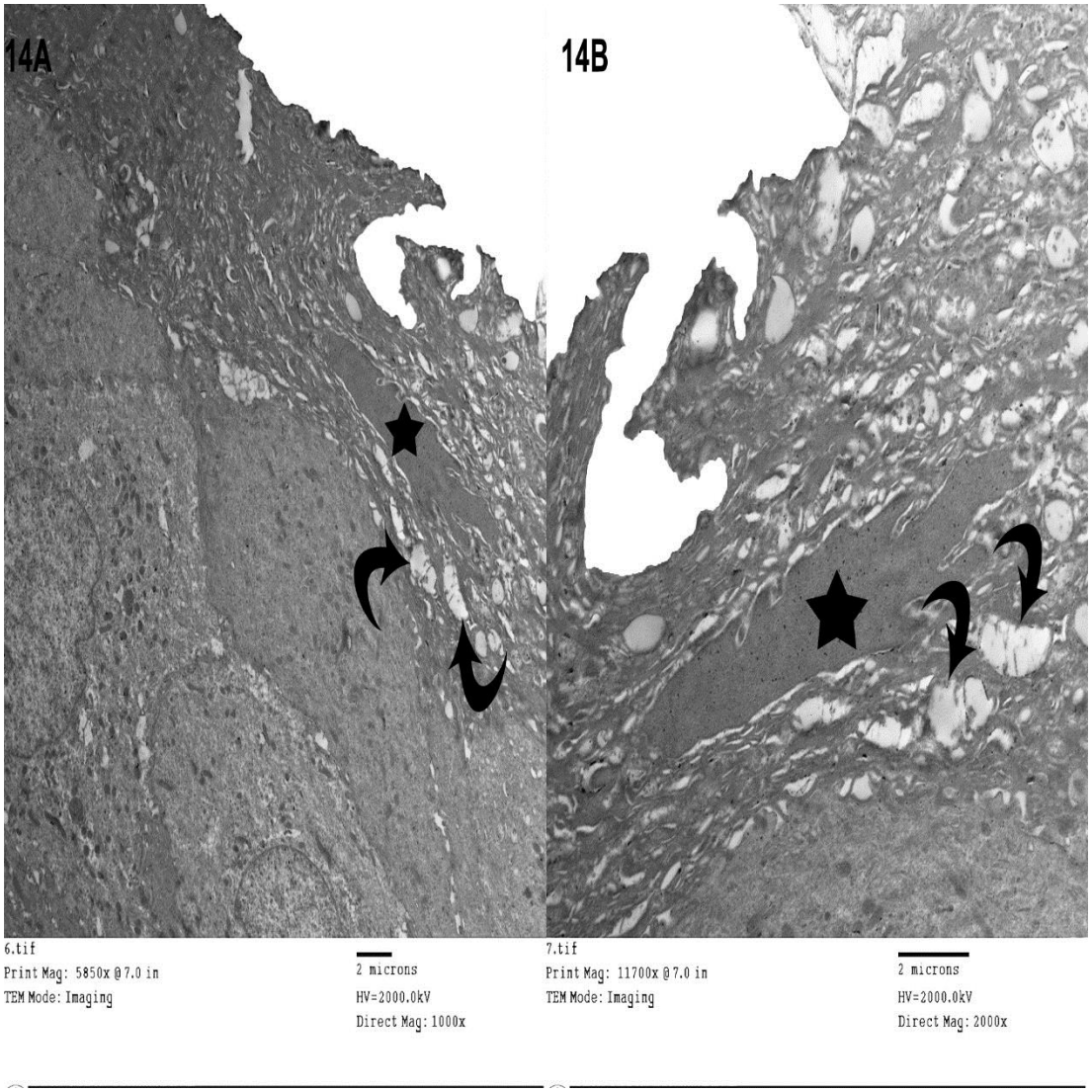

Fig. (14- A&B): Electron micrographs of the urothelium from HC group showing dark shrunken nucleus **(star)** with cytoplasmic vacuolation **(curved arrows)**. **(X 1000, X 2000)**.

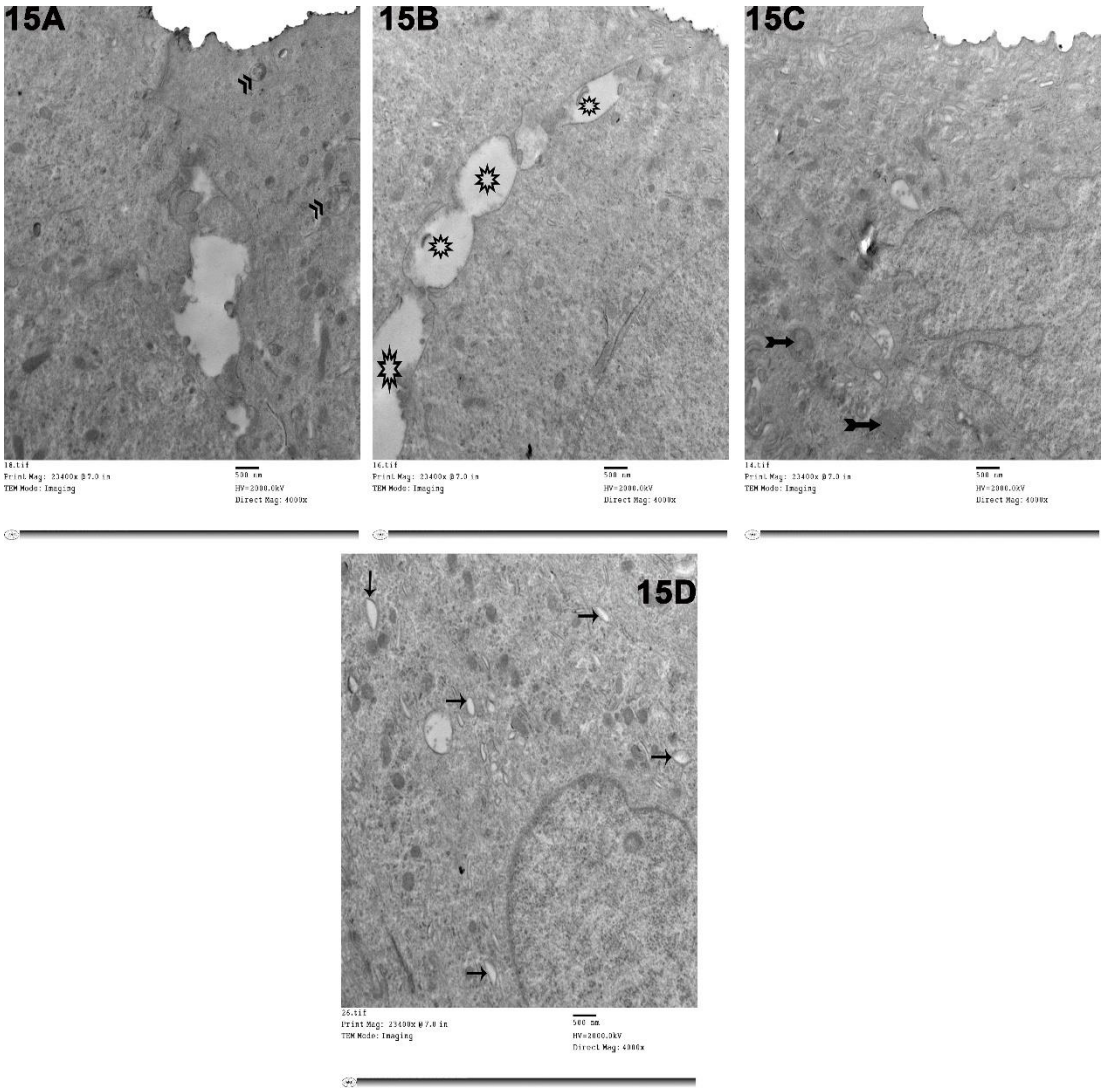

Fig. (15): An electron micrograph of the urothelium from HC group. **15-A)** showing presence of secondary lysozyme **(double headed arrow). 15-B)** showing widening of the intercellular space **(star). 15-C)** showing swollen mitochondria **(bifid arrows). 15-D)** showing dilated RER **(black arrows). (X 4000)**.

Fig. (16): An electron micrograph of the urothelium from HC group. **16-A)** showing discontinuity of basement membrane **(white bifid arrows) (X 4000)**. **16-B)** showing excessive deposition of the collagen bundles **(zigzag arrow)**. **16-C)** showing large, congested blood capillary in the lamina propria **(BV) (X 1000)**.

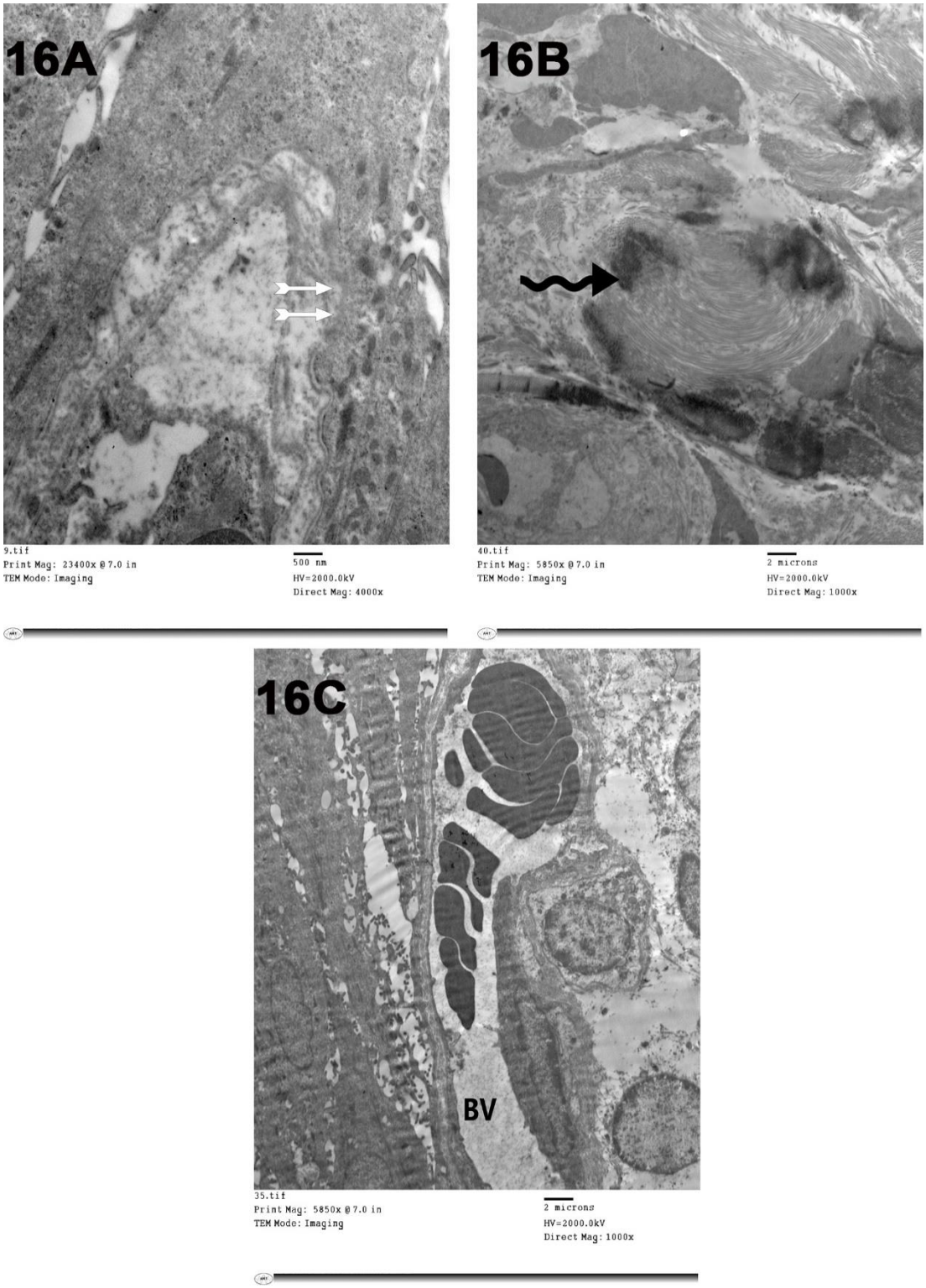

Fig. (16): An electron micrograph of the urothelium from HC group. **16-A)** showing discontinuity of basement membrane **(white bifid arrows) (X 4000)**. **16-B)** showing excessive deposition of the collagen bundles **(zigzag arrow)**. **16-C)** showing large, congested blood capillary in the lamina propria **(BV) (X 1000)**.

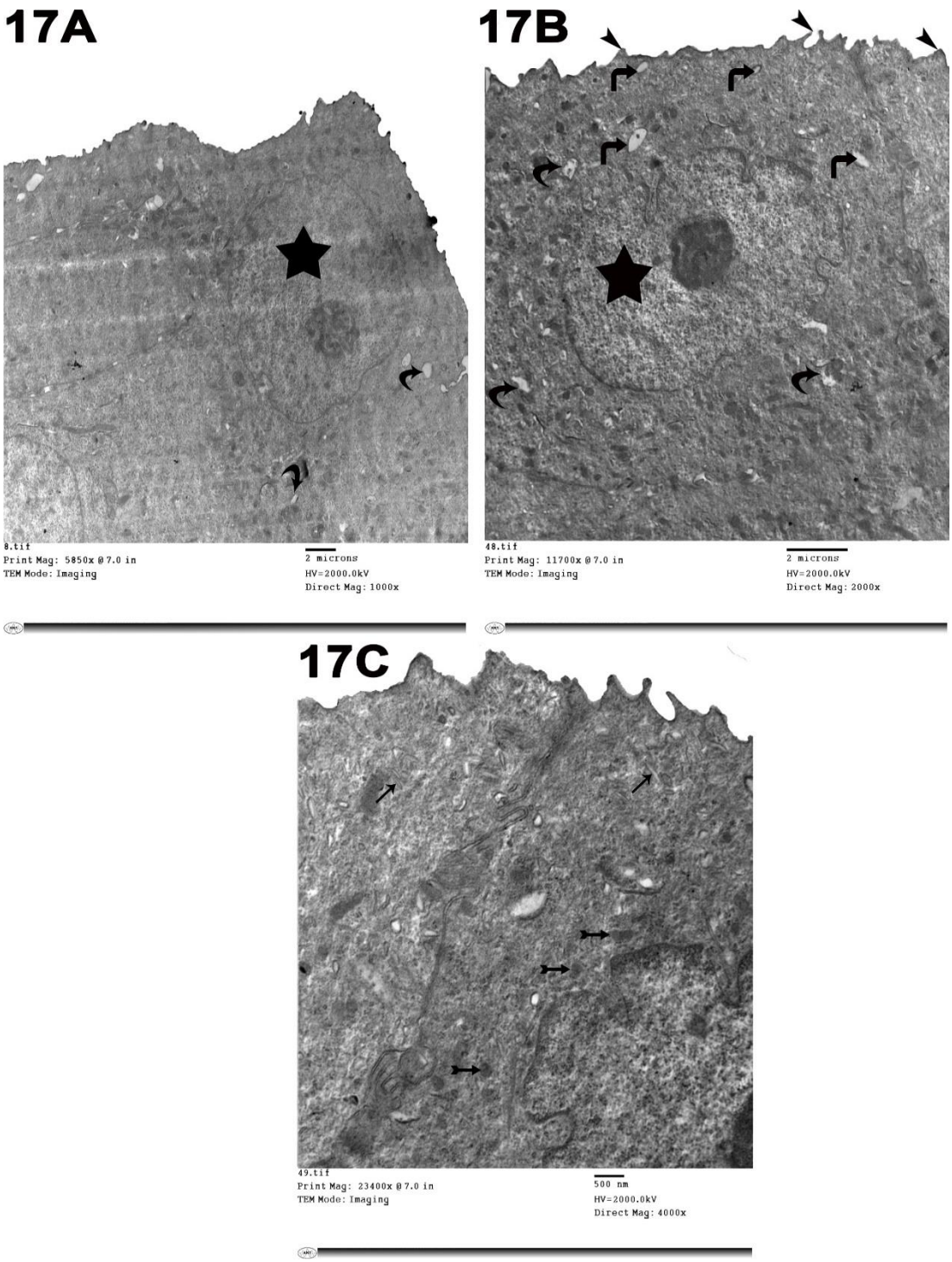

Fig. (17): An electron micrograph of the urothelium of PSO-HC group. **17-A)** showing nucleus with prominent nucleolus **(star)** and few cytoplasmic vacuolation **(curved arrows) (X 1000)**. **17-B)** showing indented nucleus **(star)** and few cytoplasmic vacuolation **(curved arrows)**. The apical contour (**arrowhead)** and apical fusiform vesicles **(bended arrows)** are also noticed **(X 2000)**. **17-C)** showing apparently normal RER **(black arrows)**, mitochondria **(bifid arrows) (X 4000).**

4. Discussion:

The present work was done to study the effect of the CYP on the histological structure of the urinary bladder of adult male albino rat and to evaluate the possibility of protective effect of PSO. This study showed that CYP drug induces histological changes in the urinary bladder. On the other hand, most of these changes were minimized using PSO.

Ibrahim et al.[17] reported that one of the mechanisms for CYP toxicity is the production of acrolein (ACR). They also documented in their research that acrolein activates the intracellular ROS and nitric oxide production that results in cell death. Additionally**, Haiba & Ibrahim.**[18] illustrated the pathogenesis and mechanisms of CYP-induced HC. He reported that there is an increase in cytokines production leading to induction of release of inducible nitric oxide synthase (INOS) that leading to occurrence of cystitis.

The present study revealed injured, desquamated and damaged urothelium. This was illustrated by **Aboulhoda et al.** [19] who suggested that CYP causes oxidative stress & increase expression of INOS in the urothelial cells, in turn, that results in occurrence of urothelial ulcer, injury and damage. This explanation goes in line with **Haiba & Ibrahim.**[18] **& Elsisy et al.** [20] who also attributed the cause of the cell damage to the oxidative stress.

Widening of intercellular space and damaging of the tight junction in H&E and ultrathin sections of the HC group were observed in this study. These data were similar to **Elabd et al.**[12] & **Essawy et al.**[21] who obtained these results in their research about CYP-treated rats. **Essawy et al.** [21] attributed the cause of the disturbed junction to the marked reduction of the E-caderin (epithelial calcium dependent adhesion molecule that is very important for maintaining inter-cellular adhesion and cell-cell contact.

PAS-stained sections of HC group revealed discontinuous & faint reaction of the GAG layer, that was confirmed by morphometric results and statistical analysis. These results coincide with **Rooney et al.**[22] **& Abdelmoez**[23] who illustrated the very important role of GAG in the urothelium. **Abdelmoez**[23] illustrated in his research about ketamine induced interstitial cystitis that the presence of GAG layer in the luminal surface of urinary bladder umbrella cells is highly important as it prevents the urinary bladder solutes to come in contact with urothelium, so any damage in the GAG layer will increase the umbrella cell permeability to the urea, that will result in

toxic effect in the bladder urothelium including GAG layer.

An apparent thinning of epithelium was noticed in H&E sections of group III. This was clarified by **Awadallah et al.** [24] who stated that the thinning of epithelium is directly related to direct contact CYP metabolites and bladder mucosa. However, other sections revealed occurrence of hyperplasia, that agreed with **Zupančič et al.** [25] who reported in their research about hyperplasia of the urothelium induced by CYP drug that CYP repeated intraperitoneal doses cause urothelial hyperplasia up to ten layers. Furthermore, they mentioned that CYP drug caused production of severe hyperplasia following the damage of the urothelium. Besides that, they mentioned that urothelium hyperplasia is accompanied by an increased number of apoptotic cells and transformation to tumor might occur. Moreover, squamous cell lining the surface of hyper proliferated urothelium, may be a sign of squamous metaplasia that may be induced by CYP metabolite called phosphramide mustard as reported by **Chou et al.** [26]

Some sections of HC-group revealed hyper eosinophilia that indicated increased cell swelling and water content inside as reported by **Chaitanya et al.** [27]. Furthermore, neovascularization was noticed in H&E sections of HC group. This goes in line with **Batista et al.** [28] who attributed the cause of neovascularization to the effect of CYP metabolites (acrolein) (ACR). Remarkably, most of H&E, semithin &ultrathin sections revealed the presence of cytoplasmic vacuolation. **Khorwal et al.**[29] mentioned that vacuolation is a sign of apoptosis that occurs due to the direct toxic effect of CYP.

H&E, semithin and ultrathin sections of group III showed many nuclear degenerative changes including karyolysis, karyorrhexis and pyknosis. These data were in agreement with **Bashandy & Zedan**[30] who attributed the cause of irregular nuclear shape to cytoskeletal proteins damage. **Attia et al.**[31] explained in his research about CYP-induced cardiotoxicity that the nuclear changes were attributed to the damage of DNA and oxidative stress.

The current study revealed excessive collagen deposition in the Masson trichrome stained sections of the HC groups, this was confirmed by statistical analysis of the area percentage of collagen deposition. These results go in line with the findings of **Bashandy & Zedan**[30] who illustrated in their research about CYP- induced cardiotoxicity that fibrosis could occur due to deposition of collagen either due to overactivity of fibroblasts to produce collagen or

reduction in collagen degradation by matrix metalloproteinase. They added that CYP causes severe inflammation resulting in fibrosis. Moreover, **Iqubal et al.**[32] added that CYP causes induction of tumor growth factor beta (TGF-β) that stimulates the transformation of fibroblast to myofibroblast. They illustrated that the myofibroblast was unique for pathological condition.

The immunostained sections of the present work showed increase of apoptotic reaction in the cytoplasm of urothelial cells of group III. This goes in line with morphometric study that revealed increased the apoptotic reaction in the HC group. **Kassab**[10] mentioned that apoptosis occurred due to changes occurred in expressions of caspases, P53, Bax, Bcl2. Bax belongs to the Bcl2 family and plays a pro-apoptotic role. **Iqubal et al.**[32] illustrated the mechanism of apoptosis and added that apoptosis is marked by occurrence of changes in the pro-apoptotic genes like bax. The pro-apoptotic proteins were activated by release of ROS, the occurrence of inflammation and oxidative stress, that resulted in bax translocation to the outer mitochondrial membrane and alteration of mitochondrial membrane permeability. These changes caused the release of cytochrome c into cytosol with subsequent activation of the apoptotic pathway.

Our results revealed an apparent disruption of basement membrane that appeared in (PAS & ultrathin sections) of HC group. **Meng et al.** [33], **Abdelmoez**[23] & **Brossard et al.** [34] mentioned in their research related to induction of cystitis that damage in the GAG layer and tight junction allow the urine to escape across the urothelial and sub urothelial layer causing damage to them. Furthermore, **Brossard et al.**[34] added that the damage of the urothelium (by urine escape effect) resulted in loss of the uroplakins and E-cadherin, in turn that cause abnormality in the urothelium polarity and architecture leading to disruption of basement membrane and the subepithelial connective tissue.

H&E sections and ultrathin sections of HC group revealed presence of dilated congested blood vessels with presence of wide space in lamina propria indicating edema. The occurrence of these findings is due to production of tumor necrotic factor-α (TNF-α), vascular endothelial growth factor (VEGF), as these factors cause an increase of vascular permeability of the endothelial cells. [34,35]

A hemorrhage was noticed in H&E sections of group III. The occurrence of hemorrhage is related to CYP metabolites acrolein, phosphramide mustard and pro inflammatory mediator cytokine (TNF-α).[19,30] Ultrathin sections of HC group

revealed RBCS in the lumen, besides that the H&E sections revealed disruption of the endothelium of the blood vessels. **Abdelmoez**[23] mentioned that disruption of blood vessels in the lamina propria occurred due to the escaped urine that will disrupt the vessels of lamina propria.

Cellular infiltration was also noticed in the H&E sections of group III of the current work. **Bashandy & Zedan**[30] mentioned that the presence of focal areas of mononuclear cellular infiltration was also noticed in HC group which indicated the occurrence of inflammation. Moreover, **Abdelmoez**[23] reported that the extravasation of inflammatory cells is due to disrupted blood vessels. Furthermore, **Jaber & Tawfeek**[36] & **Almeida de Oliveira et al.**[37] suggested that the cause of cellular infiltration is due to TNF-α, VEGF and ROS as these factors increase the vascular permeability causing escape of the inflammatory cells.

Examination of semithin section of HC group revealed mast cell infiltration into various layer of urothelium that coincided with **Abdelmoez**[23] who illustrated role of mast cells in cystitis, that the mast cell activation exacerbates the inflammation caused from cystitis. She also added that the degree of cystitis is correlated with the degree of mast cell infiltration into urothelium. Also, the author mentioned that extravasation of mast cells occurs due to disruption of blood vessels.

Our H&E sections of HC group revealed muscle changes including muscle damage and muscle disorganization with wide space in-between muscle fibers, these finding go in line with **Aboulhoda et al.** [19] & **Attia et al.** [31] who attributed the histological changes of urinary bladder musculosa to inflammatory effect of CYP drug and the attraction of the inflammatory cells into the urinary bladder wall.

Electron microscopic examination of sections of HC group revealed presence of swollen mitochondria. **Kassab & Tawfik**[38] mentioned in their research about energy drink-treated rats that swollen disrupted mitochondria was a manifestation of cell damage. **Attia et al.** [31] reported that the mitochondrial damage and these changes occurred due to susceptibility of mitochondria to the oxidative stress more than other cell organelles leading to mitochondrial dysfunction and decreasing the activity of the enzymes of the mitochondria.

Another electron microscopic findings were detected as dilated endoplasmic reticulum and multiple secondary lysosomes. **Iqubal et al.** [32] attributed ER changes to toxic metabolites produced by CYP like acrolein. **Abonar et al.** [39] attributed presence of secondary lysosome to increase of the autophagy.

They illustrated that ROS release with lipid peroxidation occurrence required the lysosomes presence and lysosomal hydrolytic enzyme activation.

At the protective level, the administration of PSO concomitant with CYP showed evident improvement in the structural changes of the urinary bladder induced by the CYP. The protective effect of PSO was also documented by **Omar & Sarhan[40], Hamdi [41] Kassab et al.[42]** who proved that PSO had strong protective effect in their research.

PSO contains important acids and minerals like linoleic and linolenic acids, beta-carotene, lutein, beta- and gamma-tocopherol, selenium and phytosterols that make PSO plays an important role in alleviation of inflammation and edema. Furthermore, PSO plays important role in reduction of cellular infiltration and decreasing the collagen fibers deposition that was mentioned by **Omar & Sarhan[40]** who stated that polyphenols and other bioactive phytochemical substances presenting in PSO play very important role as anti-inflammatory substances.

Moreover, PSO is very rich with essential fatty acids and polyunsaturated fatty acids (linoleic acid, oleic acid, palmitic acid, omega 3, 6 and 9, carotenes), that play important role in alleviation of inflammation and reduction of lipid peroxidation that was mentioned by**[43].** Furthermore, PSO helps the preservation of polyunsaturated fatty acids and the phospholipids of cell membrane. It also protects the cell membrane from the harmful effect of the peroxyl-radicles. This mechanism was explained by **Kassab et al.[42]** in their research about the role of PSO in orlistat-induced tongue mucosal damage.

Tocopherols and selenium (components of the pumpkin) play an important role in prevention of GSH depletion and have role as antioxidants. **Andrade et al.[44]** mentioned that selenium plays a very important role as it enters in the structure of an enzyme called glutathione peroxidase (GPx) which protects cells from harmful effects.

Bardaa et al.[45] reported that PSO plays an important role in wound healing and in cellular injuries that occurred due to scavenging effect of PSO against superoxidase, and hydroxyl and peroxy-radicals. They also suggested a cause for healing effect of PSO by helping the blood clotting, it also shortens the bleeding time and provides a hemostatic effect. Polyphenols and fatty acids are very important in reduction of the endothelial damage that occurred due to effects of inflammatory mediators as reported by **Hussain et al.[46]**

According to the previous findings, it

could be concluded that CYP-induced damaging effects on the histological structure of the urinary bladder structure of adult male albino rats and PSO could to some extent ameliorates these effects most probably through its antioxidants and anti-inflammatory effects. So, PSO administration in concomitant with CYP is recommended for people who are susceptible to CYP-toxicity.

5. Conclusion and Recommendations:

Based on the current study and from all previously mentioned results, PSO administration decreases CYP-induced HC. So, it could be useful for prevention and treatment of hemorrhagic cystitis. Further studies are needed to study the role of GAG layer in urinary bladder inflammation and to extend the experimental data to clinical application. Meanwhile, adjusting the specific concentration of PSO in different clinical conditions should be considered.

Conflicts of interest

There are no conflicts of interest.

6. References:

1. **Mbanefo, E. C., Le, L., Zee, R., Banskota, N., Ishida, K., Pennington, L. F., Odegaard, J. I., Jardetzky, T. S., Alouffi, A., & Falcone, F. H. (2019).** IPSE, a urogenital parasite-derived immunomodulatory protein, ameliorates ifosfamide-induced hemorrhagic cystitis through downregulation of pro-inflammatory pathways. *Scientific Reports*, *9*(1), 1586,1-14.
2. **Swan, D., Gurney, M., Krawczyk, J., Ryan, A. E., & O'Dwyer, M. (2020).** Beyond DNA damage: exploring the immunomodulatory effects of cyclophosphamide in multiple myeloma. *Hemasphere*, *4*(2), e350,1-10.
3. **Zhang, Z., Pan, T., Liu, C., Shan, X., Xu, Z., Hong, H., Lin, H., Chen, J., & Sun, H. (2021).** Cyclophosphamide induced physiological and biochemical changes in mice with an emphasis on sensitivity analysis. *Ecotoxicology and Environmental Safety*, *211*, 111889,1-6.
4. **Elmeligy, M. H., Farid, A. S., and Fararh, K. (2019):** Antioxidant and hepatoprotective effect of pumpkin seed oil in CCl4-intoxicated rats. Benha Veterinary Medical Journal, 36(2): 77-89.
5. **Hamdi, H., and Hassan, M. M. (2021**): Maternal and developmental toxicity induced by nanoalumina administration in albino rats and the potential preventive role of the pumpkin seed oil. Saudi Journal of

Biological Sciences, 28(8): 4778-4785.

6. **Dobrek, L., Nalik-Iwaniak, K., Fic, K., & Arent, Z. (2020).** The effect of acetylcysteine on renal function in experimental models of cyclophosphamide-And ifosfamide-induced cystitis. Current Urology, 14(3), 150–162.
7. **El-Azma, M. H., El-Beih, N. M., El-Shamy, K. A., Koriem, K. M. M., Elkassaby, M. I., & El-Sayed, W. M. (2022).** Pumpkin seed oil and zinc attenuate chronic mild stress perturbations in the cerebral cortex of rats. Nutrition & Food Science, 52(7), 1070–1082.
8. **Ghasi, S. I., Umana, I. K., Ogbonna, A. O., Nwokike, M. O., & Ufelle, S. (2020).** Cardioprotective effects of animal grade piperazine citrate on isoproterenol induced myocardial infarction in wistar rats: Biochemical and histopathological evaluation. African Journal of Pharmacy and Pharmacology, 14(8), 285–293.
9. **Suvarna, K.S., Layton, C. and Bancroft, J.D. (2013):** Bancroft's Theory and Practice of Histological Techniques. 7th edition, Elsevier, Churchill Livingstone, chapters 6-12, pp:105-224.
10. **Kassab, A. A. (2018).** Wheat germ oil attenuates deltamethrin-induced injury in rat cerebellar cortex: Histological and immunohistochemical study. Egyptian Journal of Histology, 41(2), 182–191.
11. **Magaki, S., Hojat, S. A., Wei, B., So, A., & Yong, W. H. (2019).** An introduction to the performance of immunohistochemistry. Biobanking: Methods and Protocols, 289–298.
12. **Elabd, S. S., Ibrahim, M. A., & Sadek, M. T. (2022).** Effect of Tadalafil on Apoptosis and Proliferation in Urinary Bladder Mucosa after Chemically Induced Hemorrhagic Cystitis; A Histological and Immunohistochemical Study. Egyptian Journal of Histology, 45(1), 1–16.
13. **Suvarna, K.S., Layton, C. and Bancroft, J.D. (2019):** Bancroft's Theory and Practice of Histological Techniques (Eighth ed.): Elsevier Health Sciences.China, chapter 21, Transmission electron microscopy. P:434-440.
14. **El Shaer, D. F., & Elkelany, M. M. (2023).** Adverse Effect of Dexamethasone on the Thyroid Gland of Adult Male Albino Rat and the Possible Protective Role of Curcumin: Histological, Immunohistochemical and Biochemical Study. *Egyptian Journal of Histology*, *46*(2), 619–634.
15. **Mahmoud, M. S. (2020).**

Gastroprotective activity of olive leaves extract on 2, 3, 7, 8 tetrachlorodibenzo-p-dioxin induced gastric fundic mucosal injury in adult male albino rats (light and electron microscopic study). *Egyptian Journal of Histology*, *43*(4), 1188–1204.

16. **Davis, H.T. and Crombie, L.K (2009):** What are confidence intervals and p-values?. 2nd edition, Hayward Group Ltd, London, United Kingdom. P: 1-6.
17. **Ibrahim, K. M., Darwish, S. F., Mantawy, E. M., & El-Demerdash, E. (2023).** Molecular mechanisms underlying cyclophosphamide-induced cognitive impairment and strategies for neuroprotection in preclinical models. *Molecular and Cellular Biochemistry*, 1–21.
18. **Haiba, D. A., & Ibrahim, M. A. A. (2015).** Role of dexamethasone alone and in combination with quercetin in the urinary bladder after administration of ifosfamide: a histological, immunohistochemical, and morphometric study. *Egyptian Journal of Histology*, *38*(2), 196–209.
19. **Aboulhoda, B. E., Amin, S. N., Thomann, C., Youakim, M., & Hassan, S. S. (2020).** Effect of thymoquinone on cyclophosphamide-induced injury in the rat urinary bladder. Archives of Medical Science, 16(1),1-12. DOI:10.5114/aoms.2020.97061.
20. **Elsisy, R. A., Taha, M. F., Sonpol, H. M. A., Baokbah, T. A. S., Abdelkareem, M. A., & Farage, A. E. (2021).** Acute effect of cyclophosphamide on rat's urinary bladder and the possible protective role of sulforaphane: a histological and ultrastructural study. International Journal of Scientific Reports, 7(4), 207-214.
21. **Essawy, A. S., Issa, N. M., & Tayel, S. G. (2022).** Glycyrrhiza glabra root extract alleviates cyclophosphamide induced mucositis of the tongue in adult male albino rats. Egyptian Journal of Histology, 45(4), 1222–1234.
22. **Rooney, P., Srivastava, A., Watson, L., Quinlan, L. R., & Pandit, A. (2015).** Hyaluronic acid decreases IL-6 and IL-8 secretion and permeability in an inflammatory model of interstitial cystitis. Acta Biomaterialia, 19, 66–75.
23. **Abdelmoez, W. A. (2022).** Evaluation of the Protective Role of Intravesical Chondroitin Sulfate Versus Intravesical Dimethyl Sulfoxide on The Glycosaminoglycan's, Uroplakin and Restoration of Barrier Function of the Urinary Bladder in A Rat model of

Ketamine Induced Interstitial C. Egyptian Academic Journal of Biological Sciences, D. Histology & Histochemistry, 14(2), 201–214.

24. **Awadallah, N., Proctor, K., Joseph, K. B., Delay, E. R., & Delay, R. J. (2020).** Cyclophosphamide has long-term effects on proliferation in olfactory epithelia. *Chemical Senses*, *45*(2), 97–109.
25. **Zupančič, D., Vidmar, G., & Jezernik, K. (2009).** Melatonin prevents the development of hyperplastic urothelium induced by repeated doses of cyclophosphamide. Virchows Archiv, 454, 657–666.
26. **Chou, W. H., McGregor, B., Schmidt, A., Carvalho, F. L. F., Hirsch, M. S., Chang, S. L., Kibel, A., & Mossanen, M. (2021).** Cyclophosphamide-associated bladder cancers and considerations for survivorship care: A systematic review. *Urologic Oncology: Seminars and Original Investigations*, *39*(10), 678–685.
27. **Chaitanya, G. V., Eeka, P., Munker, R., Alexander, J. S., & Babu, P. P. (2011).** Role of cytotoxic protease granzyme-b in neuronal degeneration during human stroke. *Brain Pathology*, *21*(1), 16–30.
28. **Batista, C., Mota, J., Souza, M. L. P., Leitão, B. T. A., Souza, M., Brito, G. A. C., Cunha, F. de Q., & Ribeiro, R. A. (2007).** Amifostine and glutathione prevent ifosfamide-and acrolein-induced hemorrhagic cystitis. Cancer Chemotherapy and Pharmacology, 59, 71–77.
29. **Khorwal, G., Chauhan, R., Nagar, M., & Khorwal, G. (2017).** Effect of cyclophosphamide on liver in albino rats: A comparative dose dependent histomorphological study. International Journal of Biomedical and Advance Research, 8(3), 102–107.
30. **Bashandy, M. A., & Zedan, O. I. (2019).** Role of alpha lipoic acid on cyclophosphamide induced cardiotoxicity in adult male albino rat: Histological study. Egyptian Journal of Histology, 42(4), 888–899.
31. **Attia, A. A., Sorour, J. M., Mohamed, N. A., Mansour, T. T., AlEisa, R. A., & El-Shenawy, N. S. (2023).** Biochemical, Histological, and Ultrastructural Studies of the Protective Role of Vitamin E on Cyclophosphamide-Induced Cardiotoxicity in Male Rats. Biomedicines, 11(2), 390, 1-14. https://doi.org/10.3390/biomedicines11020390.
32. **Iqubal, A., Iqubal, M. K., Sharma, S., Ansari, M. A., Najmi, A. K., Ali, S. M., Ali, J., & Haque, S. E. (2019).**

Molecular mechanism involved in cyclophosphamide-induced cardiotoxicity: Old drug with a new vision. Life Sciences, 218, 112–131.

33. **Meng, E., Hsu, Y., & Chuang, Y. (2018).** Advances in intravesical therapy for bladder pain syndrome (BPS)/interstitial cystitis (IC). *LUTS: Lower Urinary Tract Symptoms*, *10*(1), 3–11.
34. **Brossard, C., Lefranc, A.-C., Pouliet, A.-L., Simon, J.-M., Benderitter, M., Milliat, F., & Chapel, A. (2022).** Molecular Mechanisms and Key Processes in Interstitial, Hemorrhagic and Radiation Cystitis. Biology, 11(7), 972, 1-18. https://doi.org/10.3390/biology11070972.
35. **Sherif, I. (2020)**. Uroprotective mechanisms of natural products against cyclophosphamide-induced urinary bladder toxicity: A comprehensive review. *Acta Scientiarum Polonorum Technologia Alimentaria*, *19*(3), 333–346.
36. **Jaber, F. A., & Tawfeek, S. El. (2023).** The Potential Ameliorative Effect of Bone Marrow Derived Mesenchymal Stem Cells on Cyclophosphamide Injured Lung in Adult Female Albino Rats. Egyptian Journal of Histology, 46(1), 448–459.
37. **Almeida de Oliveira, L. S., de Moura Bandeira, S. R., Gomes Gonçalves, R. L., Pereira de Sousa Neto, B., Carvalho de Rezende, D., dos Reis-Filho, A. C., Sousa, I. J. O., PinheiroNeto, F. R., Timah Acha, B., & do Nascimento Caldas Trindade, G. (2022).** The isopropyl gallate counteracts cyclophosphamide-induced hemorrhagic cystitis in mice. Biology, 11(5), 728, 1-17. https://doi.org/10.3390/biology11050728.
38. **Kassab, A. A., & Tawfik, S. M. (2018).** Effect of a caffeinated energy drink and its withdrawal on the submandibular salivary gland of adult male albino rats: A histological and immunohistochemical study. Egyptian Journal of Histology, 41(1), 11–26.
39. **Abonar, M., Aboraya, A., Elbakary, N., & Elwan, W. (2022).** Effect of Energy Drink on the Pancreas of Adult Male Albino Rat and the Possible Protective Role of Avocado Oil. Histological and Immunohistochemical Study. Egyptian Journal of Histology, 45(2), 386–403.
40. **Omar, N. M., & Sarhan, N. R. (2017).** The possible protective role of pumpkin seed oil in an animal model of acid aspiration pneumonia: Light

and electron microscopic study. Acta Histochemica, 119(2), 161–171.

41. **Hamdi, H. (2020).** Testicular dysfunction induced by aluminum oxide nanoparticle administration in albino rats and the possible protective role of the pumpkin seed oil. The Journal of Basic and Applied Zoology, 81, 1–12.
42. **Kassab, A. A., Moustafa, K. A. A., & Abd-El-Hafez, A. A. (2020).** The possible protective role of pumpkin seed oil in ameliorating tongue mucosal damage induced by orlistat in adult male albino rats: A light and scanning electron microscopic study. Egyptian Journal of Histology, 43(4), 975–987.
43. **Ofoego, U. C., Nweke, E. O., & Orji, C. (2019).** Co-Administration of Cyclophosphamide and Ethanolic Seed Extract Of Telfairia Occidentalis (Pumpkin) Protects Testicular Functions In Adult Male Albino Wistar Rats. World Journal of Pharmaceutical Research, 8(3), 325–342.
44. **Andrade, I. G. A., Suano-Souza, F. I., Fonseca, F. L. A., Lago, C. S. A., & Sarni, R. O. S. (2021).** Selenium levels and glutathione peroxidase activity in patients with ataxia-telangiectasia: association with oxidative stress and lipid status biomarkers. Orphanet Journal of Rare Diseases, 16, 1–10.
45. **Bardaa, S., Ben Halima, N., Aloui, F., Ben Mansour, R., Jabeur, H., Bouaziz, M., & Sahnoun, Z. (2016).** Oil from pumpkin (Cucurbita pepo L.) seeds: evaluation of its functional properties on wound healing in rats. Lipids in Health and Disease, 15, 1–12.
46. **Hussain, A., Kausar, T., Sehar, S., Sarwar, A., Quddoos, M. Y., Aslam, J., Liaqat, A., Siddique, T., An, Q. U., & Kauser, S. (2023).** A review on biochemical constituents of pumpkin and their role as pharma foods; a key strategy to improve health in post COVID 19 period. Food Production, Processing and Nutrition, 5(1), 22, 1-14. https://doi.org/10.1186/s43014-023-00138-z.